The Journal of Neuroscience

https://jneurosci.msubmit.net

JN-RM-2463-21R1

Electrophysiological validation of monosynaptic connectivity between premotor interneurons and the aCC motoneuron in the Drosophila larval CNS.

Richard Baines, The University of Manchester Faculty of Biology Medicine and Health
Carlo Giachello, University of Manchester
Iain Hunter, University of Manchester
Tom Pettini, University of Cambridge
Bramwell Coulson, University of Manchester
Athene Knufer, University of Cambridge
Sebastian Cachero, University of Cambridge
Michael Winding, University of Cambridge
Aref Arzan Zarin, Texas A&M University
Hiroshi Kohsaka, Denki Tsushin Daigaku
Yuen Ngan Fan, University of Manchester
Akinao Nose, Tokyo Daigaku
Matthias Landgraf, Department of Zoology University of Cambridge

Commercial Interest:

Electrophysiological validation of monosynaptic connectivity between premotor interneurons and the aCC motoneuron in the *Drosophila* larval CNS.

Validating connections between *Drosophila* neurons

Carlo N. G. Giachello[1†] and Iain Hunter[1†], Tom Pettini[2], Bramwell Coulson[1], Athene Knufer[2], Sebastian Cachero[3], Michael Winding[2], Aref Arzan Zarin[4], Hiroshi Kohsaka[5], Yuen Ngan Fan[1], Akinao Nose[6], Matthias Landgraf[2] and Richard A. Baines[1]*

[1]Division of Neuroscience and Experimental Psychology, School of Biological Sciences, Faculty of Biology, Medicine and Health, University of Manchester, Manchester Academic Health Science Centre, Manchester, M13 9PL, UK.

[2]Department of Zoology, University of Cambridge, Cambridge, CB2 3EJ, UK.

[3]Neurobiology Division, MRC Laboratory of Molecular Biology, Cambridge CB2 0QH, UK.

[4]Department of Biology, Texas A&M University, College Station, United States.

[5]Graduate School of Informatics and Engineering, The University of Electro-Communications, 1-5-1, Chofugaoka, Chofu-shi, Tokyo, 182-8585, Japan.

[6]Department of Complexity Science and Engineering, Graduate School of Frontier Sciences, University of Tokyo, Tokyo, Japan.

[†]Joint first authors

*Corresponding author:

Email: Richard.Baines@manchester.ac.uk

Number of pages: 32 (including title pages and references)

Number of figures: 10

Number of tables: 1

Number of words for: (1) Abstract, 249; (2) Sig. Statement, 112; (3) Introduction, 749; (4) Discussion, 989 (excluding table).

Author Contributions

C.N.G.G., I.H., M.L. and R.A.B. designed research. C.N.G.G., I.H., T.P., A.K., B.C., Y.N.F. and M.L. performed research. B.C., A.A.Z, H.K., Y.N.F., A.N., M.L., S.C. and M.W. contributed unpublished reagents/ analytic tools. C.N.G.G., I.H., A.K., T.P. and Y.N.F. analysed data. C.N.G.G., I.H. and R.A.B. wrote the paper. I.H., A.A.Z., M.L. and R.A.B. edited the paper.

Conflicts of interest

The authors declare no competing financial interests.

Acknowledgements

We thank Chris Doe for generous provision of GAL4 lines and for advice in conducting this study, and Jan Felix Evers for designing a cyan fluorescent version of GRASP. This work was supported by funding from the Biotechnology and Biological Sciences Research Council to R.A.B. (BB/N/014561/1) and to M.L. (BB/R016666/1) and by a Joint Wellcome Trust investigator award to R.A.B. and M.L. (217099/Z/19/Z). S.C. was supported by a Dorothy Hodgkin Fellowship from the Royal Society to S.C. (DH120072), and benefitted from core support from the MRC (MC-U105188491). Work on this project benefited from the Manchester Fly Facility, established through funds from the University and the Wellcome Trust (087742/Z/08/Z), and from the Imaging Facility, Department of Zoology, supported by Dr. Matthew Wayland and funds from a Wellcome Trust Equipment Grant (WT079204) with contributions by the Sir Isaac Newton Trust in Cambridge, including Research Grant (18.07ii(c)).

Present address for C.N.G.G is Syngenta, Jealott's Hill International Research Centre, Bracknell, RG42 6EY, United Kingdom. Present address for Y.N.F. is Unit 2 & 2a Enterprise House, Lloyd Street North, Manchester, M15 6SE, United Kingdom.

1 Abstract

The *Drosophila* connectome project aims to map the synaptic connectivity of entire larval and adult fly neural networks, which is essential for understanding nervous system development and function. So far, the project has produced an impressive amount of electron microscopy data that has facilitated reconstructions of specific synapses, including many in the larval locomotor circuit. While this breakthrough represents a technical *tour-de-force*, the data remain under-utilised, partly due to a lack of functional validation of reconstructions. Attempts to validate connectivity posited by the connectome project, have mostly relied on behavioural assays and/or GRASP or GCaMP imaging. While these techniques are useful, they have limited spatial or temporal resolution. Electrophysiological assays of synaptic connectivity overcome these limitations. Here, we combine patch clamp recordings with optogenetic stimulation in male and female larvae, to test synaptic connectivity proposed by connectome reconstructions. Specifically, we use multiple driver lines to confirm that several connections between premotor interneurons and the anterior corner cell (aCC) motoneuron are, as the connectome project suggests, monosynaptic. In contrast, our results also show that conclusions based on GRASP imaging may provide false positive results regarding connectivity between cells. We also present a novel imaging tool, based on the same technology as our electrophysiology, as a favourable alternative to GRASP. Finally, of eight Gal4 lines tested, five are reliably expressed in the premotors they are targeted to. Thus, our work highlights the need to confirm functional synaptic connectivity, driver line specificity, and use of appropriate genetic tools to support connectome projects.

2 Significance Statement

The *Drosophila* connectome project aims to provide a complete description of connectivity between neurons in an organism that presents experimental advantages over other models. It has reconstructed over 80 percent of the fly larva's synaptic connections by manual identification of anatomical landmarks present in serial section transmission electron microscopy (ssTEM) volumes of the larval CNS. We use a highly reliable electrophysiological approach to verify these connections, so provide useful insight into the accuracy of work based on ssTEM. We also present a novel imaging tool for validating excitatory monosynaptic connections between cells, and show that several genetic driver lines designed to target neurons of the larval connectome exhibit non-specific and/or unreliable expression.

3 Introduction

Invertebrate models are often used for experiments on neural circuits, because they offer several advantages over mammals (Hunter et al., 2021). One is the large number of 'identified neurons' in invertebrates, which occupy reliable anatomical positions across preparations. This is important for work that combines cell-specific genetic manipulation with electrophysiology in *Drosophila* (Baines and Bate, 1998, Baines et al., 1999, Baines et al., 2002, Baines et al., 2001, Ryglewski et al., 2012, Srinivasan et al., 2012a, Srinivasan et al., 2012b, Worrell and Levine, 2008, Kadas et al., 2017, Choi et al., 2004). Indeed, identified neurons are amenable to cell type-specific genetic manipulation via 'driver lines', such as split-GAL4 lines (Kohsaka et al., 2014, Schneider-Mizell et al., 2016, Fushiki et al., 2016, Hasegawa et al., 2016, Kohsaka et al., 2019). It is therefore significant that recently, the entire *Drosophila* first-instar larval nervous system was imaged using serial section transmission electron microscopy (ssTEM, (Gerhard et al., 2017, Larderet et al., 2017, Saumweber et al., 2018, Schneider-Mizell et al., 2016, Zarin et al., 2019, Ohyama et al., 2015)) and annotated into a CATMAID (Saalfeld et al., 2009) dataset. This dataset is being used by the *Drosophila* connectome project to identify all neurons in the larval CNS, and to characterise the connections between them. The project has already reconstructed the majority of the CNS, and a large number of putative

105 neuronal connections has been published (Kohsaka et al., 2014, Heckscher et al., 2015, Itakura et al.,
106 2015, Fushiki et al., 2016, Hasegawa et al., 2016, Schneider-Mizell et al., 2016, Yoshikawa et al.,
107 2016, Zwart et al., 2016, Burgos et al., 2018, Carreira-Rosario et al., 2018, Zarin et al., 2019).
108 Researchers are making use of this information and cell type-associated transgenic expression lines, to
109 investigate the physiology and function of neurons and neural networks (Giachello et al., 2019,
110 Ackerman et al., 2021, Giachello et al., 2021). The accuracy of this and future work is, therefore,
111 predicated on the accuracy of manual reconstructions conducted as part of the connectome project,
112 and the expression patterns of related driver lines. Both may be subject to error, and require
113 validation.

114 Most attempts to validate connections posited by ssTEM reconstruction have focused on behavioural
115 analysis and/or functional imaging using GRASP or GCaMP, which can suggest that activity is co-
116 ordinated across neurons (Kohsaka et al., 2019, Zarin et al., 2019, Hasegawa et al., 2016). However,
117 the value of using these techniques to validate synaptic connectivity, is limited by a lack of spatial or
118 temporal resolution that makes it difficult to determine whether cells are mono-, or polysynaptically
119 connected. Given this limitation, a combination of optogenetics, Ca^{2+}-imaging and pharmacology has
120 been used to determine monosynaptic connectivity (Sales et al., 2019). However, results generated by
121 this approach may be complicated by variability in responses recorded from the postsynaptic neuron.
122 In contrast, electrophysiology provides unambiguous evidence for monosynaptic connections between
123 cells, and is regarded as the 'gold standard' for doing so. It is perhaps surprising then, that few
124 publications have used electrophysiology to functionally validate a connection posited in the
125 connectome (Fushiki et al., 2016). This may be due to the difficulty of the technique, and
126 corresponding paucity of researchers able to employ it.

127 In this study, we used a whole-cell patch-clamp electrophysiology-based assay for connectivity, to
128 validate connections posed by connectome project reconstructions. Specifically, we screened Gal4
129 driver lines that were reported to target expression of Gal4 to five identified premotor interneurons:
130 cholinergic A27h, A18a (a.k.a. CLI2) and A18b3 (a.k.a. CLI1), plus GABAergic A23a and A31k.
131 These interneurons were proposed to monosynaptically connect to the anterior corner cell motoneuron

(aCC, a.k.a. MN1-lb (Hoang and Chiba, 2001)), however, this connectivity had not been functionally validated prior to the present work. We adapted a protocol called 'TERPS' (Zhang and Gaudry, 2016), which uses genetically-targeted expression of a tetrodotoxin(TTX)-insensitive bacterial cation channel, NaChBac (Ren et al., 2001), to test whether neurons are monosynaptically connected (Zhang and Gaudry, 2018, Suzuki et al., 2020) and showed that four of the five premotor interneurons are connected to aCC. We also highlighted the limitations of GRASP, which has been shown previously and in the present research, to infer a direct connection between A18b3 and aCC (Hasegawa et al., 2016). This contrasts the more accurate results we generated using TERPS, which demonstrate that this is not the case. Finally, we show that not all Gal4 lines express as suggested by name, so highlight the importance of careful characterisation of expression before lines are used to infer cell or network function.

4 Materials and methods

4.1 Experimental design

4.1.1 Drosophila rearing and stocks

All *Drosophila* stocks were kept on standard corn meal medium, at 25$^{\circ C}$. The following lines provided the optogenetic and other transgenic tools necessary to manipulate and record connectivity of neurons: *ChR; NaChBac* (*w*; 20xUAS- T159C-ChR2; UAS-NaChBac-EGFP / TM6C*^{Sb,Tb}), which was created by crossing *y*^{1}*,w*; PBac{20xUAS-ChR2.T195C-HA}VK00018; Dr*^{1}*/ TM6C*$^{Sb, Tb}$ (#52258, Bloomington *Drosophila* Stock Center (BDSC), Indiana, USA) and *y*^{1}*,w*; P{UAS-NaChBac-EGFP}1/ TM3*^{Sb} (#9467, BDSC); *w*; UAS-H134R-ChR2;* + (gift from Stefan Pulver) and *w*; P(y[+t7.7] w*; P{20xUAS-Chronos-mVenus}attP40* (#77115, BDSC). These lines were also combined with one expressing an RCaMP transgene (described in section *4.1.2.*) to produce the imaging tool for assessing monosynaptic connectivity between neurons: *w[*]; DvGlut-T2A-QF2, P{y[+t7.7], 5xQUAS IVS syn21 RCaMP1b P2A nls-GFP P10 in su(Hw)attP5, 20xUAS-ChR2.T159C-HA}VK00018/ CyO, Dfd-GMR-YFP; UAS-NaChBac-EGFP}1 in 85A & 87D/ TM6b*^{Sb}*, Dfd-GMR-YFP*.

Driver lines targeting Gal4 expression to interneurons were: *w*^{1118}*; +; R36G02*-Gal4 ("A27h-Gal4", #49939, BDSC), which expresses in the premotor interneuron A27h, as well as in three other neurons (Fushiki et al., 2016); *w*^{1118}*; +; 47E12*-Gal4 (CLIs-Gal4, #50317, BDSC), which expresses in A18b3 (a.k.a. CLI1) and A18a (a.k.a. CLI2), plus a range of other interneurons and some sensory neurons (Hasegawa et al., 2016); *w*$^{-}$*; +; R47E12*-Gal4*; cha3.3*-Gal80 ("CLI1/2-Gal4"), which exploits Gal80 to facilitate more specific expression to A18b3 and A18a, than *47E12*-Gal4 does alone (Hasegawa et al., 2016); *w*$^{-}$*; tsh*-Gal80*; R47E12*-Gal4*; cha3.3*-Gal80 ("CLI1-Gal4"), which is specific for A18b3 (Hasegawa et al., 2016); *w*$^{-}$*; +; R15B07*-Gal4 ("CLI2-Gal4"), which is specific for A18a (Hasegawa et al., 2016); *w*$^{-}$*; +; GAD1-T2A*-Gal4 expresses in all GABAergic neurons (Diao et al., 2015). We used three driver lines reported to express in the GABAergic premotor interneuron, A23a: *R78F07*-Gal4 (Zarin et al., 2019), *R78F07*-AD*; R49C08*-DBD split Gal4 and *R41G07*-AD*; R78F07*-DBD split Gal4 (a.k.a. *SS04495*-Gal4, (Kohsaka et al., 2019)). We also used three driver lines reported to express in the GABAergic premotor interneuron, A31k: *R87H09*-Gal4 (Zarin et al., 2019), *R20A03*-AD*; R87H09*-DBD split Gal4 (unpublished) and *R20A03*-AD*; R93B07*-DBD split Gal4 (a.k.a. *SS04399*-Gal4, (Kohsaka et al., 2019)). For cyan GRASP experiments, we used the following line: *w*-; UAS-CD4::spCer1-10, LexAop-CD4::spGFP11/CyO, *Dfd*-GMR-YFP; RN2-FLP (hopA), tub-FRT-stop-FRT-LexA::VP16, 13xLexAop2-myr::YPet (attP2)/TM6b, *Sb*, *Dfd*-GMR-YFP, and line *y*^{1} *w**; P{w[+mC]=UAS-CD4-tdTom}7M1 (#35841, BDSC).

4.1.2 ***Molecular biology***

To generate a cyan fluorescent version of GRASP, four mutations (Y66W, S72A, H148D and N149I) were introduced into the 1-10 fragment of spGFP. The mutated sequence was codon optimised and synthesised by IDT. PAT2-SP::Cerulean1-10 and CD2 coding sequences, as well the pJFRC161 vector backbone, were PCR amplified, all with overlapping ends, then ligated via gibson assembly. Flies were transformed by BestGene.

183 Cerulean1-10 coding sequence:

184 ATGTCCAAGGGCGAGGAGCTGTTCACCGGCGTGGTGCCCATCCTGGTGGAGCTGGACGG
185 CGACGTGAACGGCCACAAGTTCTCCGTGCGCGGCGAGGGCGAGGGCGACGCCACCATCG
186 GCAAGCTGACCCTGAAGTTCATCTGCACCACCGGCAAGCTGCCCGTGCCCTGGCCCACCC
187 TGGTGACCACCCTGACCTGGGGCGTGCAGTGCTTCGCCCGCTACCCCGACCACATGAAGC
188 GCCACGACTTCTTCAAGTCCGCCATGCCCGAGGGCTACGTGCAGGAGCGCACCATCTCCT
189 TCAAGGACGACGGCAAGTACAAGACCCGCGCCGTGGTGAAGTTCGAGGGCGACACCCTG
190 GTGAACCGCATCGAGCTGAAGGGCACCGACTTCAAGGAGGACGGCAACATCCTGGGCCA
191 CAAGCTGGAGTACAACTTCAACTCCGACATCGTGTACATCACCGCCGACAAGCAGAAGA
192 ACGGCATCAAGGCCAACTTCACCGTGCGCCACAACGTGGAGGACGGCTCCGTGCAGCTG
193 GCCGACCACTACCAGCAGAACACCCCCATCGGCGACGGCCCCGTGCTGCTGCCCGACAA
194 CCACTACCTGTCCACCCAGACCGTGCTGTCCAAGGACCCCAACGAGAAGGGCACC.

195 Primers used: Cerulean1-10fwd,
196 GAAACGACTAACCCTAATTCTTATCCTTTACTTCAGGCGGCCGCGGCTCGAGCAGATATC
197 GACAAGTTTGTAC; Cerulean1-10rev, CTCTGCAGTCAGTTGTGGTGCCCTTCTCGTTG;
198 CD2fwd, CACCACAACTGACTGCAGAGACAGTGGGAC; CD2rev,
199 CCAATTATGTCACACCACAGAAGTAAGGTTCCTTCACAAAGATCCTCTAGACACCACTTT
200 GTACAAGAAAGCTG; pJFRC161fwd, TCTAGAGGATCTTTGTGAAGGAAC; pJFRC161rev,
201 CTCGAGCCGCGGCCGCCTGAAGTAAAG.

202 To generate the *5xQUAS-IVS-syn21-RCaMP1b-P2A-nls::GFP-P10* transgene necessary for the
203 RCaMP imaging tool for assessing monosynaptic connectivity between neurons, we used a
204 commercial gene synthesis (GenScript) for the insert and upstream activation sequence, followed by
205 restriction enzyme-based cloning into the pJFRC7 backbone (Pfeiffer et al., 2010), whose 20xUAS
206 sequences were replaced with 5xQUAS (Potter et al., 2010). Within the bicistronic insert, the red-
207 shifted calcium indicator with nuclear export sequence (NES-jRCaMP1b (Dana et al., 2016)) is
208 separated from EGFP with a nuclear localization sequence by the self-cleaving peptide sequence P2A
209 (Kim et al., 2011, Daniels et al., 2014). Three translational enhancers (IVS, Syn21, and p10) were

added to 5' or 3' untranslated regions (UTR) (Pfeiffer et al., 2012). A fly stock was then generated by inserting this construct into the su(Hw)attP5 landing site using phiC31 site-specific recombination (Groth et al., 2004).

4.1.3 ***Gal4 expression and GRASP imaging***

Newly-hatched male and female larvae containing one copy of the GAL4 producing transgene(s) and 10xUAS-IVS-myr::GFP transgene reporter inserted in attP2 (Pfeiffer et al., 2010) were kept on apple juice agar plates with yeast paste food, at 25°C until the third instar stage of development (48 hrs after larval hatching (ALH)). Each larva was dissected in extracellular saline to isolate the CNS, using a hypodermic syringe needle (30G - BD Microlance) as a scalpel. The CNS was then transferred onto poly-L-lysine-coated (Sigma) cover glass, and fixed with 4% paraformaldehyde (Agar Scientific) in saline for 15 minutes, at room temperature. Following the standard procedures of washes in phosphate buffered saline (PBS) containing 0.3% Triton X-100 and 0.25% (w/v) bovine serum albumin (BSA, Sigma), Gal4-directed expression of membrane-targeted GFP was visualised in the longitudinal Fasciclin II-positive axon tracts (Landgraf et al., 2003) via Chicken anti-GFP (ab13970, Abcam at 1:5,000), visualised with Donkey anti-Chicken-CF488A (20166, Biotium, at 1:1,000) and mouse anti-Fasciclin II (1D4, DSHB at 1:20), visualised with Goat anti-Mouse-StarRed (Abberior, at 1:2,000). Stained nerve cords were cleared in 70% glycerol, then mounted in EverBrite medium (Biotium, Cambridge BioScience) and sandwiched under a second cover glass, with thin aluminium foil strips used as spacers. Imaging was performed with one of two confocal point scanning microscopes: a Leica SP5 with a 63x/1.2 NA glycerol immersion objective, or an Olympus FV3000 with a 60x/1.3 NA silicone oil immersion objective.

For imaging GRASP, male and female larvae were dissected in extracellular saline (135mM NaCl, 5mM KCl, 4mM $MgCl_2 \cdot 6H_2O$, 2mM $CaCl_2 \cdot 2H_2O$, 5mM TES and 36mM sucrose, pH 7.15) to isolate the ventral nerve cord (VNC) and brain lobes. This preparation was placed on a poly-L-lysine (Sigma) coated coverglass, dorsal side up, and imaged immediately using a custom built spinning disk confocal field scanning system consisting of: a CSU-22 field scanner (Yokagawa), mounted on a

fixed stage upright Olympus microscope frame (BX51-WI), equipped with a single objective piezo focusing device (Physik Instruments); a 60x/1.2 NA water immersion objective (Olympus), external filter wheel (Sutter) and programmable XY stage (Prior). Images were acquired at an effective voxel size of 0.217 × 0.217 × 0.3 µm using a back-thinned Evolve EMCCD camera (Photometrics), operated via MetaMorph software (Molecular Devices).

4.1.4 ***Electrophysiology***

Electrophysiological recordings were performed as previously described (Baines et al., 1990, Marley and Baines, 2011), in mostly third (L3) or occasionally first (L1) instar larvae (as relevant to Results). In brief, the protocol for assessing monosynaptic connectivity between neurons was as follows: male and female larvae were dissected as for imaging GRASP signal, and the isolated CNS preparation was glued to a Sylgard-coated cover slip on a slide. Prior to recording, interneuron Gal4 and GFP-tagged reporter line expression (for example, 'CLI2'-Gal4 x *UAS-T159C-ChR2; UAS-NaChBac-EGFP*) was checked by momentarily exposing preparations to blue light (470nm LED (bandwidth 25nm, irradiance 15.62mW·cm^{-2}; OptoLED, Cairn Instruments, Kent, UK)), while viewing them under an Olympus BX51WI microscope (Olympus Corporation, Tokyo, Japan). Once expression was confirmed, aCC motoneurons present in the VNC segment(s) that expressed the interneuron Gal4 and reporter, were identified using bright-field microscopy. Protease (Sigma, Poole, UK) was applied to those segments to remove overlaying glia, to facilitate access to aCC for patching. 2µM TTX was pipetted directly into the extracellular saline and given ~60s to diffuse across the preparation, unless the experiment was a TTX-free control. Other drugs (10µM picrotoxin (PTX), 1mM gabazine or 167-200µM mecamylamine) were used to abolish responses observed in the presence TTX, so were pipetted into the extracellular saline following a first, and prior to a second optogenetic stimulation protocol (see below).

Whole-cell voltage or current-clamp recordings were made from A27h or aCC, using thick-walled borosilicate glass pipettes (GC100F-10, Harvard Apparatus, Edenbridge, UK) that were fire polished to resistances of 10-15MΩ (for L3 aCC) or 15-20MΩ (L1 aCC or L3 A27h) and filled with

262 intracellular saline (140mM K^+-D-gluconate, 2mM $MgCl_2 \cdot 6H_2O$, 2mM EGTA, 5mM KCl, and 20mM
263 HEPES, pH 7.4). KCl, $CaCl_2$, $MgCl_2$ and sucrose used to make extracellular and/ or intracellular
264 saline were from Fisher Scientific (Loughborough, UK). All other chemicals were from Sigma.
265 Recordings were made using a Multiclamp 700B amplifier controlled by pCLAMP (version 10.4), via
266 a Digidata 1440A analog-to-digital converter (Molecular Devices, Sunnyvale, CA). Traces were
267 sampled at 20 kHz and filtered online at 10 kHz. Once the "whole cell" conformation was achieved,
268 input resistance was measured, and only cells with an input resistance ≥0.5 GΩ and V_m ≤-40mV were
269 used for experiments.

270 Voltage-clamp recordings were performed at -60mV for excitatory, and -40mV for inhibitory
271 interneurons (A27h, A18a, A18b3 and A23a, A31k, respectively), to promote and standardise driving
272 force to ensure reliable inputs to aCC. Inputs were elicited by optogenetic stimulation of the
273 interneuron, and amplitude of input was calculated as the change in current (pA, normalised for cell
274 capacitance, determined by integration of the area under a capacity transient generated by a -60 to -
275 90mV step protocol) from baseline to peak, following stimulation. Excitation of ChR was achieved
276 using a 470nm LED connected to the microscope. Light output was controlled by Clampex (version
277 10.4) and was pulsed onto the preparation for 1s, per one sweep. Specifically, the Clampex
278 stimulation protocol was 5 sweeps (repetitions) of 1s LED off, 1s LED on, 1s off, for each
279 preparation.

280 Current-clamp recordings were made by injecting current (~10pA) sufficient to evoke action
281 potentials in aCC, at a frequency of ~3-8Hz. Cells were then subjected to the same optogenetic
282 stimulation used for voltage-clamp experiments (1s LED off, 1s on, 1s off), to assess the impact of
283 interneuron input on aCC firing frequency. Frequency was calculated as the number of action
284 potentials occurring during the 1s before, during and after optogenetic stimulation.

285

4.1.5 ***RCaMP imaging***

Male and female larvae were dissected and mounted as for electrophysiology, and 2μM TTX was added to the saline droplet and left to incubate for 5 minutes. The preparation was positioned under a 40x water immersion lens on an Olympus BX51WI microscope (Olympus Corporation, Tokyo, Japan) and Gal4-UAS expression (e.g. 'A27h'-Gal4 driving *UAS-NaChBac-EGFP*) was confirmed as it was for electrophysiology (momentary exposure to 470nm light). Imaging was recorded through excitation filters #378827 and #348474, plus a #378710 barrier filter (Chroma Technology Cop, Vermont, USA) by a Hamamatsu ORCA-Flash4.0 digital camera, at a frame rate of 10Hz, in Winflour V4.1.5. 470nm light was used to stimulate ChR and depolarise premotor interneurons expressing Gal4, while 590nm light was used to visualise RCaMP activity in aCC. Activity was imaged for 60-430s, with the 590nm LED switched off between stimulations for longer recordings, to prevent bleaching fluorophores. After imaging, ROIs were drawn around aCC soma present in segments in which premotor interneuron Gal4 was expressed. The fluorescence changes observed in these ROIs were normalised to an ROI positioned in a dark area of the image(s), quantified in arbitrary units (AUs), then exported to ClampFit (version 10) to generate data traces.

4.1.6 ***Drugs***

TTX was from Alomone Labs, Israel. PTX, gabazine (SR95531) and mecamylamine were from Sigma.

4.2 ***Statistical analysis***

Electrophysiology data was imported into Microsoft Excel (Microsoft Corp., Redmond, WA) and statistical tests were performed in GraphPad Prism (version 7, GraphPad Software, San Diego, CA). Statistical tests were not applied to measurements of synaptic inputs or RCaMP imaging, due to the descriptive nature of this data. Conversely, repeated measures one-way ANOVA with Bonferroni's *post-hoc* multiple comparisons tests were applied to firing plots, to quantify premotor drive to aCC. P values < 0.05 were considered significant, and levels of significance were represented by: * = P <

0.05, ** = $P < 0.01$. Comparisons that did not reach significance are not marked. Figures were edited to improve presentation, in Adobe Illustrator CS3 (Adobe, San Jose, CA, USA).

5 Results

5.1 Validating the NaChBac tool and confirming A27h is monosynaptically connected to aCC

We adapted 'TERPS' (Zhang and Gaudry, 2016), which exploits the insensitivity of the voltage-gated sodium channel from *Bacillus halodurans* (NaChBac) to TTX (Ren et al., 2001), to demonstrate that NaChBac-expressing neurons are monosynaptically connected to postsynaptic cells (Zhang and Gaudry, 2016, Zhang and Gaudry, 2018, Suzuki et al., 2020). We generated a transgenic stock containing both *UAS-NaChBac* and the T159C variant of *UAS-Channelrhodopsin (ChR)* (Berndt et al., 2011), to allow them to be expressed simultaneously. Crossing this stock to interneuron-specific Gal4 lines and recording optogenetically-induced synaptic drive in the postsynaptic aCC motoneuron, in the presence of TTX, therefore demonstrates monosynaptic connectivity between cells (Figure 1).

We validated our tool by crossing it to *R36G02*-Gal4 (Fushiki et al., 2016), which is expressed in a number of INs, including A27h (Figure 2A). Prior to the current work, A27h was the only IN that possessed a connection to aCC predicted by network reconstruction, which had been verified by electrophysiology (Fushiki et al., 2016). Whole-cell patch-clamp recordings from A27h expressing ChR and NaChBac, demonstrated the functional properties of the latter. As expected, optogenetic stimulation of A27h induced a large and slowly-inactivating depolarisation that is characteristic of NaChBac conductance, in the presence of 2μM TTX (arrowhead in Figure 3A, left panel). Importantly, evoked action potential firing in A27h (arrow in Figure 3A, right panel) is absent in the presence of TTX (Figure 3B). Depolarisation of A27h via injection of constant current (1pA steps/ 0.5s) showed that NaChBac activates at -65 ± 12mV (Figure 3B). The rate of inactivation of NaChBac increases steeply as a function of voltage (Ren et al., 2001), so we determined NaChBac steady-state inactivation by measuring the peak amplitude of the current activated by ChR (470nm, 1s), (Figure 3C). This showed that NaChBac activity is severely reduced at prepulse membrane

potentials more positive than -40mV (Figure 3D), which is consistent with NaChBac expressed in CHO-K1 cells (Ren et al., 2001). This severe reduction in activity at > -40mV should be considered when planning and interpreting experiments using this tool (see Discussion).

5.2 ***A18a but not A18b3, is monosynaptically connected to aCC***

The A18a and A18b3 interneurons (originally named CLI2 and CLI1, respectively) were first identified by their rhythmic activity, which correlates with locomotion (Hasegawa et al., 2016). We tested four different Gal4 lines that have been reported to express in A18a and A18b3, in the trunk of the nerve cord: *R47E12*-Gal4, a.k.a. 'CLIs-Gal4', targets A18a and A18b3, some uncharacterised interneurons, plus some sensory neurons; *R47E12*-Gal4*; cha3.3*-Gal80, a.k.a. *'CLI1/2*-Gal4*'*, is only expressed in A18a and A18b3 (Hasegawa et al., 2016); *tsh*-Gal80*; R47E12*-Gal4*, cha3.3*-Gal80, a.k.a. 'CLI1-Gal4', is specific for A18b3 (Hasegawa et al., 2016) and *R15B07*-Gal4, a.k.a. 'CLI2-Gal4', which is specific for A18a (Figure 2B). Perhaps unsurprisingly, the most broadly expressed line, *R47E12*-Gal4 ("CLIs-Gal4"), provided the largest synaptic drive to aCC in the absence of TTX. This drive is notably reduced, but not fully blocked, by TTX (-9.55 ± 3.19pA/pF, n = 4, to -3.57 ± 0.92pA/pF, n = 6, Figure 4A-C). The fact that stimulation of *R47E12*-Gal4-expressing neurons is more excitatory before application of TTX than after, suggests that additional neurons (besides A18a and A18b3) express Gal4, and are directly or indirectly connected to aCC.

Our results using *R47E12*-Gal4*; cha3.3*-Gal80 ("CLI/2-Gal4") and *R15B07*-Gal4 ("CLI2-Gal4") demonstrated a decrease in synaptic drive in the presence vs. the absence of TTX. Currents recorded using *R47E12*-Gal4*; cha3.3*-Gal80 decreased from -3.59 ± 1.10pA/pF (n = 5) to -1.25 ± 0.55pA/pF (n = 10), while those recorded using *R15B07*-Gal4 dropped from -2.74 ± 1.09pA/pF (n = 5) to -1.49 ± 0.73pA/pF (n = 6). Interestingly, we recorded similar current amplitudes following depolarisation of *R47E12*-Gal4*; cha3.3*-Gal80 and *R15B07*-Gal4-expressing neurons, which suggests that A18a (CLI2) provides the majority of the excitatory presynaptic input to aCC. This was confirmed by the fact that optogenetically stimulating A18b3 (CLI1) using *tsh*-Gal80*; R47E12*-Gal4*, cha3.3*-Gal80, did not provide synaptic drive to aCC, neither in the absence nor presence of TTX (-0.09 ± 0.09pA/pF, n = 8, to -0.01 ± 0.01pA/pF, n = 9). Thus, we conclude that A18a, but not A18b3, is monosynaptically

connected to aCC. This is in agreement with the description in (Zarin et al., 2019), and suggests *R15B07*-Gal4 is the most accurate and reliable Gal4 line to use for testing 'CLI' input to aCC.

5.3 ***aCC receives GABAergic inputs***

The connectome identifies inhibitory neurons making direct synaptic connections to motoneurons, including aCC (Kohsaka et al., 2019). In contrast, however, to the single cholinergic connection (A27h to aCC) that was established before our work was conducted (Fushiki et al., 2016), none of the proposed GABAergic inputs had been validated by electrophysiology. We therefore began by attempting to demonstrate GABAergic input to aCC, by expressing NaChBac in all GABAergic neurons (*GAD1-T2A*-Gal4). Widespread expression of NaChBac driven by *GAD1-T2A*-Gal4 was lethal, so we expressed ChR in GABAergic neurons instead, and recorded the synaptic input to aCC. aCC is not tonically active, so we injected current to evoke AP firing, prior to optogenetic stimulation. Activation of GABAergic neurons produced a significant decrease in AP firing in aCC ($F_{(2, 18)} = 8.391$, $P = 0.0137$, repeated measures one-way ANOVA) for the duration of the light pulse (8.89 ± 1.85 to 0.35 ± 0.24, $n = 7$, $P = 0.0103$, Bonferroni's post hoc test, Figure 5A). Firing resumed shortly after cessation of light stimulation (4.26 ± 2.75 *vs.* 8.89 ± 1.85, $n = 7$, $P = 0.1166$, Bonferroni's post hoc test). As further evidence for inhibitory drive, voltage-clamp traces showed increasing synaptic current density as aCC was depolarised away from the chloride reversal potential. A current of +0.25 ± 0.13 pA/pF ($n = 8$) at -60 mV increased, as expected for Cl^- ions, to +1.65 ± 0.36 pA/pF ($n = 8$) in the same cells at -40 mV (Figure 5B-C). Similarly, current-clamp recordings clearly exhibited an increasing hyperpolarising drive to aCC of -1.93 ± 0.80 mV and -6.56 ± 1.18 mV, at -60 mV, or -40 mV, respectively (Figure 5D-E).

5.4 ***A23a is monosynaptically connected to aCC***

A23a was first described as a GABAergic interneuron presynaptic to the aCC motoneuron, which is active during both forward and backward peristaltic waves (Kohsaka et al., 2019). We tested three Gal4 lines reported to express in A23a: *R78F07*-Gal4 (Zarin et al., 2019); *R78F07*-AD*; R49C08*-DBD split Gal4 (unpublished); and *R41G07*-AD *78F07*-DBD split Gal4, a.k.a. *SS04495*-Gal4 (Kohsaka et al., 2019).

We found that optogenetic activation of *R78F07*-Gal4-expressing neurons usually caused a decrease in AP firing ($F_{(2, 15)} = 5.005$, $P = 0.0216$, repeated measures one-way ANOVA), consistent with an inhibitory input to aCC (4.70 ± 1.07 *vs.* 1.32 ± 0.61 APs, $n = 6$, $P = 0.0406$, Bonferroni's post hoc test; post LED = 5.02 ± 1.01 APs, Figure 6A). *R78F07*-Gal4, however, exhibits an expression pattern that is more diverse than expected; it targets some interneurons that are not A23a (Ackerman et al., 2021). This lack of specificity is reflected in the heterogeneity of responses recorded from aCC. In the absence of TTX, inhibitory inputs prevailed (input average: -1.73 ± 1.02mV at -40mV, $n = 7$, Figure 6B), while recordings performed in the presence of TTX revealed an additional excitatory component (5 out of 8 cells). This suggests that the inhibitory input includes a contribution from neurons polysynaptically connected to aCC, and that this GAL4 expresses in monosynaptically-connected excitatory premotor interneurons (input average: -0.46 ± 0.75mV at -40mV, $n = 10$, Figure 6B). This is illustrated in Figure 6C, where the inhibitory component becomes excitatory after TTX application. In summary, our results suggest that *R78F07*-Gal4 is not selective, nor reliable, for activation of the A23a inhibitory premotor interneuron.

Next, we tested two split-Gal4 lines designed for specific expression in A23a. The first split Gal4 tested, *R78F07*-AD*; R49C08*-DBD, was predominantly expressed in thoracic segments of the ventral nerve cord (VNC). As expected, this expression appeared to be specific to A23a (see Figure 2C). Optogenetic activation of *R78F07*-AD*; R49C08*-DBD often reduced evoked action potential firing in aCC. In some experiments, however, *R78F07*-AD*; R49C08*-DBD-expressing cells excited aCC. Indeed, it did so consistently, so the mean effect of stimulation on aCC AP firing was not significant

($F_{(2, 21)} = 0.8322$, $P = 0.4005$, repeated measures one-way ANOVA; 4.78 ± 0.69 *vs*. 4.42 ± 0.90 APs, $n = 8$, $P > 0.99$, Bonferroni's post hoc test; post LED = 4.39 ± 0.68 APs, Figure 6D). This suggests that *R78F07*-AD*; R49C08*-DBD was expressed in A23a, but also in excitatory (presumed cholinergic) INs that synapse with aCC. We tested and supported this suggestion by showing *R78F07*-AD*; R49C08*-DBD input was always inhibitory when experiments were conducted in the presence of 200µM mecamylamine.

The second A23a-split line we used was *SS04495*-Gal4: *R41G07*-AD*; R78F07*-DBD (Kohsaka et al., 2019). It was predominantly expressed in abdominal segments of the VNC, however, the degree of expression in specific segments was variable (Figure 2D). Moreover, the expression pattern includes at least one neuron that is not A23a. Optogenetic activation of cells expressing *SS04495*-Gal4 led to a significant reduction in evoked AP firing in aCC ($F_{(2, 21)} = 9.662$, $P = 0.0141$, repeated measures one-way ANOVA; from 4.50 ± 0.42 to 2.16 ± 0.80 APs, $n = 8$, $P > 0.0415$, Bonferroni's post hoc test; post LED = 4.70 ± 0.54 APs, Figure 6E). The same stimulation produced a mostly reliable hyperpolarising effect on aCC that was unaffected by application of TTX (-1.88 ± 0.87 mV, $n = 10$, *vs*. -1.66 ± 0.80 mV at -40 mV, $n = 11$, -TTX *vs*. +TTX, $P = 0.8502$, *t*-test, $t_{(df\ 19)} = 0.1915$, Figure 6F). Only one of the traces shown here, and 2/6 recorded from crosses to *UAS-Chronos-mVenus*, demonstrated an excitatory effect of *SS04495*-Gal4-expressing cells on aCC (which was blocked by 200µM mecamylamine (data not shown)). *SS04495*-Gal4 is therefore more reliably associated with the expected effect of the GABAergic interneuron (A23a) on aCC, than the other lines we tested.

Finally, to support our proposal that *SS04495*-Gal4 was the most reliable of those currently available for expression in A23a, we confirmed that the inhibition we observed was due to the movement of Cl^- ions. Currents recorded from cells held at -40mV were larger than from those held at -60mV (Figure 6G), and the inhibitory effect of the A23a to aCC connection was blocked by PTX (10µM, Figure 6H) and gabazine (1mM, Figure 6I).

5.5 ***A31k is monosynaptically connected to aCC***

A31k was identified as a GABAergic IN connected to aCC (Schneider-Mizell et al., 2016) and later shown to inhibit motor activity (Clark et al., 2018, Zarin et al., 2019) downstream of 'canon' neurons (Hiramoto et al., 2021). We tested three different drivers to verify A31k to aCC connectivity: *R87H09*-Gal4 (Zarin et al., 2019); *R20A03*-AD*; R87H09*-DBD split Gal4 (unpublished) and *R20A03*-AD*; R93B07*-DBD split Gal4 (a.k.a. *SS04399*-Gal4 (Kohsaka et al., 2019)).

Evoked AP firing in aCC was not changed by optogenetic activation of A31k in the absence or presence of TTX, using either *R87H09*-Gal4 ($F_{(2, 12)} = 0.5102$, $P = 0.5559$, repeated measures one-way ANOVA; 6.73 ± 0.81 *vs*. 6.68 ± 0.90 APs, pre LED *vs*. LED, respectively, $n = 7$, $P > 0.99$, repeated measure one-way ANOVA followed by Bonferroni's post hoc test; post LED = 6.46 ± 0.90 APs, data not shown), or *R20A03*-AD*; R87H09*-DBD split Gal4 ($F_{(2, 6)} = 1.733$, $P = 0.3134$, repeated measures one-way ANOVA; 3.20 ± 0.56 *vs*. 3.53 ± 0.43 APs, pre LED *vs*. LED, respectively, $n = 3$, $P > 0.99$, Bonferroni's post hoc test; post LED = 3.73 ± 0.50 APs, Figure 7A). Similarly, voltage-clamp recordings provided no indication of input from Gal4-expressing neurons to aCC in both driver lines (data not shown). Given that our recordings were conducted in third instar animals and the connectome was generated from a first instar larva, we repeated our experiments at L1. Our results mirrored those observed at the L3 stage, with no change in evoked AP firing recorded in aCC following optogenetic stimulation of *R20A03*-AD*; R87H09*-DBD split Gal4-expressing neurons ($F_{(2, 12)} = 0.5404$, $P = 0.5928$, repeated measures one-way ANOVA; from 5.99 ± 0.97 to 5.98 ± 1.14, $n = 5$, $P > 0.99$, Bonferroni's post hoc test; post LED = 6.41 ± 0.83 APs, Figure 7B). Thus, the lack of aCC response to *R87H09*-Gal4 and *R20A03*-AD*; R87H09*-DBD spilt Gal4-expressing cell stimulation is probably not due to changes in connectivity occurring during development. It more likely reflects inaccurate and/ or unreliable expression.

In contrast to results generated using *R87H09*-Gal4 and *R20A03*-AD*; R87H09*-DBD, optogenetic activation of neurons targeted by the split-Gal4 driver line, *SS04399*-Gal4 (*R20A03*-AD*; R93B07*-DBD), produced a clear inhibition of evoked AP firing in aCC ($F_{(2, 12)} = 20.22$, $P = 0.0011$, repeated measures one-way ANOVA; from 3.66 ± 0.49 to 0.99 ± 0.37 APs, $n = 5$, $P = 0.0088$ Bonferroni's

post hoc test; post LED = 3.68 ± 0.81 APs, Figure 7C). Current-clamp recordings confirmed the presence of a hyperpolarising drive with no significant reduction after application of TTX (-2.82 ± 0.51mV, n = 10, *vs*. -2.11 ± 0.72mV at -40mV, n = 11, -TTX *vs*. +TTX, P = 0.4347, t-test, $t_{(df\ 19)}$ = 0.798, Figure 7D). Similar to A23a, optogenetic activation of A31k produces an outward current in aCC clamped at -40mV, which is reduced at -60mV (Figure 7E). Bath application of PTX (Figure 7F) or gabazine (Figure 7G) blocked this inhibition, which is consistent with it being carried by Cl^- ions. Note that *SS04399*-Gal4 is predominantly expressed in the two most posterior abdominal segments of the VNC, at 48h AEL (see Figure 2E for expression pattern). In summary, our results indicate that A31k makes a robust GABAergic, monosynaptic connection with aCC. The premotor neuron can be accurately and reliably targeted in posterior abdominal segments by the split Gal4 line, *SS04399*-Gal4: *R20A03*-AD*; R93B07*-DBD (Kohsaka et al., 2019).

5.6 TERPS is more accurate than GRASP and can be adapted for imaging excitatory monosynaptic connections between neurons

GRASP and calcium imaging represent the primary techniques by which connectivity proposed by reconstruction of neural networks, had been verified prior to the present study. This type of validation may, however, be limited by the spatial and temporal resolution of these methods. We demonstrated this limitation by direct comparison of GRASP imaging to our electrophysiology results for A18a (a.k.a. CLI2) and A18b3 (a.k.a. CLI1). Prior research used GRASP to infer "direct" connections between both A18a and A18b3 and aCC (Hasegawa et al., 2016), and using a similar system we also found GRASP-positive cell-cell contacts (see Figure 8). In contrast, the more accurate, functional connectivity assessment we made using TERPS showed that while A18a is connected to aCC, A18b3 is not (Figure 4C). Thus, GRASP should be used to indicate close apposition between cells, rather than synaptic connectivity (Couton et al., 2015).

Electrophysiology is difficult to perform and requires expensive, specialist equipment. Similarly, our research is one of very few to deploy TERPS to assess monosynaptic connectivity between neurons in *Drosophila* (Zhang and Gaudry, 2018, Suzuki et al., 2020). This difficulty and expense of electrophysiology, combined with the novel nature of our adaptation of TERPS, inspired us to design

a tool that can be used more easily to conduct similar work. Specifically, we created a stock that facilitates targeted expression of *UAS-ChR* and *UAS-NaChBac* in neurons, for testing monosynaptic input to glutamatergic neurons (including all motoneurons). In addition to ChR and NaChBac, the line expresses RCaMP1b in motoneurons (genotype: *w[*]; DvGlut-T2A-QF2, P{y[+t7.7], 5xQUAS IVS syn21 RCaMP1b P2A nls-GFP P10 in su(Hw)attP5, 20xUAS-ChR2.T159C-HA}VK00018/ CyO, Dfd-GMR-YFP; UAS-NaChBac-EGFP}1 in 85A & 87D/ TM6b*^{Sb}*, Dfd-GMR-YFP*). It can, therefore, be crossed to interneuron-specific Gal4 lines to establish monosynaptic connectivity between those (interneurons) and motoneurons by functional calcium imaging.

We validated the tool by crossing it to *R36G02*-Gal4 (A27h), and imaging calcium activity in aCC following optogenetic activation of this premotor interneuron. Stimulation of A27h, in the presence of TTX, elicited a robust change in calcium levels in aCC (n = 5, Figure 9A, left panel). As expected, application of mecamylamine (which inhibits all cholinergic synaptic transmission) abolished this response (Figure 9A, right panel), leaving only a smaller light-induced artifact produced by the blue LED used to excite ChR (see arrowhead in CS wild type controls, Figure 9C). Thus, our results validate the imaging tool by confirming those generated by electrophysiology. We also tested the potential to use the tool to establish monosynaptic connectivity between inhibitory premotor interneurons and aCC, using A31k-specific *SS04399*-Gal4 (Kohsaka et al., 2019) (Figure 9B). We were unable to validate the tool for this application, as aCC must be active prior to input from inhibitory neurons, for a noticeable change in calcium levels to be observed.

6 Discussion

In this study, we used electrophysiology to validate monosynaptic connectivity of four identified premotor interneurons with the aCC motoneuron in *Drosophila* larvae (Figure 10). Two are cholinergic and form part of the excitatory input to motoneurons, and two are GABAergic and inhibitory (Baines et al., 1999, Rohrbough and Broadie, 2002, Itakura et al., 2015, Zarin et al., 2019, Zwart et al., 2016, Fushiki et al., 2016, Kohsaka et al., 2014, Kohsaka et al., 2019). Together, they form part of a central pattern generator comprised of interneurons and motoneurons, which regulates locomotion in *Drosophila* larvae. This locomotor circuit is central to much of the work directed

517 towards establishing the fly connectome, so it is significant that our combination of electrophysiology
518 with TTX-resistant NaChBac (Zhang and Gaudry, 2018), supports certain connectome data (Zarin et
519 al., 2019). Importantly, our data also highlights the potential for inaccuracy when connectivity is not
520 validated by electrophysiology (e.g., in the case of A18b3). This confirms that electrophysiology
521 represents the 'gold standard' test for functional connectivity between neurons, and poses that it
522 should be employed to check all new connections proposed by reconstructions. It may, however, be
523 difficult to do so. Testing every synapse associated with each of the ~10,000 neurons present in the
524 larval NS (Heimbeck et al., 1999), represents an immense amount of work. It may be more practical
525 to use electrophysiology or the imaging tool we presented in this research intermittently, to confirm
526 the principles by which connections are proposed.

527 Given that the NaChBac tool presented here may be used to provide further insights into the accuracy
528 of connections predicted by the CATMAID dataset, it is important to briefly revisit the main caveat to
529 using the tool. That is, if a presynaptic neuron has a resting membrane potential of or above -40mV,
530 the NaChBac ion channel will be inactivated (Ren et al., 2001). Consequently, stimulating a
531 presynaptic cell and recording a lack of response from a supposed postsynaptic partner (in the
532 presence of TTX, which blocks endogenous Na_V channels), may be misinterpreted to mean that two
533 cells are not monosynaptically connected, when, in fact, they might be. Given that most
534 electrophysiologists do not include cells resting at <-40mV in their research (more depolarised cells
535 tend to fire spontaneous action potentials that reflect damage), this should not impact the vast majority
536 of potential applications for this tool. However, in conditions where a cell membrane potential is
537 unknown (for example, when using the imaging tool we presented), persistence of synaptic drive in
538 the presence of TTX is strong evidence for monosynaptic connectivity, but its absence is not
539 definitive evidence against it.

540 The kinetics of NaChBac are radically different to those of the endogenous Na^+ channel, Paralytic, so
541 there is little to be gained from analysing the biophysics of synaptic drive when NaChBac is
542 expressed (Baines and Bate, 1998, Baines et al., 2001, Ren et al., 2001). Another, more general issue
543 with the ectopic expression of an ion channel (particularly one of bacterial origin) in a neuron, is that

its presence may be sufficient to alter development and/or physiology (Zhang and Gaudry, 2018). Indeed, we show here that expression of NaChBac in all GABAergic neurons is embryonic lethal. This technique is also specific to detection of synaptic couplings that involve ionotropic receptors, which cause significant change to the postsynaptic membrane potential (and/or Ca^{2+} influx) and neurons that spike (i.e. excludes graded neurons). The tool cannot be applied to reliably detect synapses that rely on metabotropic receptors, which alter second messenger signalling, unless ionic movements across the neuronal membrane form part of the activated downstream signalling pathway.

GRASP has been used to validate synaptic connectivity (Sales et al., 2019, Hasegawa et al., 2016), however, we demonstrate that it is limited by poor spatial resolution (Figure 8). We therefore present an alternative, image-based tool which may be used to establish excitatory monosynaptic connections between neurons if access to electrophysiology is limited. This tool cannot identify inhibitory synapses as it is presented, however, it is conceivable that it could be adapted to do so. For example, combining the imaging tool with a high K^+ saline (or similar) that first excites postsynaptic cells, may facilitate observation of a reduction of activity due to inhibitory inputs.

In addition to identifying the most accurate and reliable Gal4s for A27h, CLI2, A23a and A31k (*R36G02*-Gal4 ("A27h-Gal4"); *R15B07*-Gal4 ("CLI2-Gal4"); *SS04495*-Gal4 ("A23a-Gal4"); *SS04399*-Gal4 ("A31k-Gal4")), we observed several that demonstrated a considerable lack of specificity and variability in the expression of different Gal4 lines, despite them targeting the same premotor interneurons (summarised in Table 1). For some (e.g. *R78F07*-Gal4), the issue was clearly the degree of specificity. Indeed, even the most accurate line for targeting Gal4 expression to A23a (*SS04495*-Gal4) must be used in conjunction with mecamylamine, to block non-specific expression from providing excitatory inputs to postsynaptic cells. For others (e.g. *R87H09*-Gal4, *R20A03*-AD; *R87H09*-DBD), the explanation for the discrepancies we observed is less apparent, but may be explained by differing strengths of Gal4 activity. It is our recommendation, therefore, that future work using relatively 'new' Gal4 lines must take time to carefully characterise their expression pattern, and confirm proposed monosynaptic connectivity using one of the tools presented in this study.

570 **Table 1. Summary of Gal4 line results**

Driver line	Other names	Target interneuron(s)	Connected to aCC	Reference
R36G02-Gal4	A27h-GAL4	A27h	✓	(Fushiki et al., 2016)
R15B07-Gal4	CLI2-GAL4	A18a	✓	(unpublished)
R47E12-Gal4	CLIs-GAL4	A18a/A18b3	✓	(Hasegawa et al., 2016)
R47E12-Gal4; cha3.3-Gal80	CLI-GAL4	A18a/A18b3	✓	(Hasegawa et al., 2016)
tsh-Gal80; *R47E12*-Gal4, cha3.3-Gal80	CLI1-GAL4	A18b3	x	(Hasegawa et al., 2016)
R78F07-Gal4		A23a	✓	(Zarin et al., 2019)
SS04495-Gal4	*R41G07*-AD; *R78F07*-DBD	A23a	✓	(Kohsaka et al., 2019)
No label	*R78F07*-AD; *R49C08*-DBD	A23a	✓	(unpublished)
SS04399-Gal4	*R20A03*-AD; *R93B07*-DBD	A31k	✓	(Kohsaka et al., 2019)
R87H09-Gal4		A31K	x	(Zarin et al., 2019)
	R20A03-AD; *R87H09*-DBD	A31K	x	(unpublished)
Confident of monosynaptic connection to aCC.				
Either no connection or possible connection, but driver not specific.				

571

572 In summary, our results validate that the premotor interneurons A27h, A18a, A23a and A31k are
573 monosynaptically connected to the aCC motoneuron, and thus confirm that the reconstructions
574 detailed in (Zarin et al., 2019) are accurate. We demonstrate that electrophysiology deserves its
575 reputation as the current 'gold standard' of validation for functional connectivity between neurons (by

contrasting it with GRASP), and, moreover, provide an imaging-based tool that others may use to verify excitatory monosynaptic connections. We identify specific GAL4 lines that are reliably and accurately expressed in A27h, A18a, A23a and A31k, so enable further study of these interneurons and their connections. This research, therefore, supports the ongoing effort to establish accurate connectomes in *Drosophila* larvae and other animals, and the development of tools for validating inter-neuronal connections.

7 References

ACKERMAN, S. D., PEREZ-CATALAN, N. A., FREEMAN, M. R. & DOE, C. Q. 2021. Astrocytes close a motor circuit critical period. *Nature*.

BAINES, R. A. & BATE, M. 1998. Electrophysiological development of central neurons in the Drosophila embryo. *J Neurosci,* 18**,** 4673-83.

BAINES, R. A., LANGE, A. B. & DOWNER, R. G. 1990. Proctolin in the innervation of the locust mandibular closer muscle modulates contractions through the elevation of inositol trisphosphate. *J Comp Neurol,* 297**,** 479-86.

BAINES, R. A., ROBINSON, S. G., FUJIOKA, M., JAYNES, J. B. & BATE, M. 1999. Postsynaptic expression of tetanus toxin light chain blocks synaptogenesis in Drosophila. *Curr Biol,* 9**,** 1267-70.

BAINES, R. A., SEUGNET, L., THOMPSON, A., SALVATERRA, P. M. & BATE, M. 2002. Regulation of synaptic connectivity: levels of Fasciclin II influence synaptic growth in the Drosophila CNS. *J Neurosci,* 22**,** 6587-95.

BAINES, R. A., UHLER, J. P., THOMPSON, A., SWEENEY, S. T. & BATE, M. 2001. Altered electrical properties in Drosophila neurons developing without synaptic transmission. *J Neurosci,* 21**,** 1523-31.

BERNDT, A., SCHOENENBERGER, P., MATTIS, J., TYE, K. M., DEISSEROTH, K., HEGEMANN, P. & OERTNER, T. G. 2011. High-efficiency channelrhodopsins for fast neuronal stimulation at low light levels. *Proc Natl Acad Sci U S A,* 108**,** 7595-600.

BURGOS, A., HONJO, K., OHYAMA, T., QIAN, C. S., SHIN, G. J. E., GOHL, D. M., SILIES, M., TRACEY, W. D., ZLATIC, M., CARDONA, A. & GRUEBER, W. B. 2018. Nociceptive interneurons control modular motor pathways to promote escape behavior in Drosophila. *Elife,* 7.

CARREIRA-ROSARIO, A., ZARIN, A. A., CLARK, M. Q., MANNING, L., FETTER, R. D., CARDONA, A. & DOE, C. Q. 2018. MDN brain descending neurons coordinately activate backward and inhibit forward locomotion. *Elife,* 7.

CHOI, J. C., PARK, D. & GRIFFITH, L. C. 2004. Electrophysiological and morphological characterization of identified motor neurons in the Drosophila third instar larva central nervous system. *Journal of Neurophysiology,* 91**,** 2353-2365.

CLARK, M. Q., ZARIN, A. A., CARREIRA-ROSARIO, A. & DOE, C. Q. 2018. Neural circuits driving larval locomotion in Drosophila. *Neural Development,* 13.

COUTON, L., MAUSS, A. S., YUNUSOV, T., DIEGELMANN, S., EVERS, J. F. & LANDGRAF, M. 2015. Development of Connectivity in a Motoneuronal Network in Drosophila Larvae. *Current Biology,* 25**,** 568-576.

DANA, H., MOHAR, B., SUN, Y., NARAYAN, S., GORDUS, A., HASSEMAN, J. P., TSEGAYE, G., HOLT, G. T., HU, A., WALPITA, D., PATEL, R., MACKLIN, J. J., BARGMANN, C. I., AHRENS, M. B., SCHREITER, E. R., JAYARAMAN, V., LOOGER, L. L., SVOBODA, K. & KIM, D. S. 2016. Sensitive red protein calcium indicators for imaging neural activity. *Elife,* 5.

619 DANIELS, R. W., ROSSANO, A. J., MACLEOD, G. T. & GANETZKY, B. 2014. Expression of Multiple
620 Transgenes from a Single Construct Using Viral 2A Peptides in Drosophila. *Plos One,* 9.
621 DHAWAN, S., MYERS, P., BAILEY, D. M. D., OSTROVSKY, A. D., EVERS, J. F. & LANDGRAF, M. 2021.
622 Reactive Oxygen Species Mediate Activity-Regulated Dendritic Plasticity Through NADPH
623 Oxidase and Aquaporin Regulation. *Frontiers in Cellular Neuroscience,* 15.
624 DIAO, F. Q., IRONFIELD, H., LUAN, H. J., DIAO, F. C., SHROPSHIRE, W. C., EWER, J., MARR, E., POTTER,
625 C. J., LANDGRAF, M. & WHITE, B. H. 2015. Plug-and-Play Genetic Access to Drosophila Cell
626 Types using Exchangeable Exon Cassettes. *Cell Reports,* 10**,** 1410-1421.
627 FUSHIKI, A., ZWART, M. F., KOHSAKA, H., FETTER, R. D., CARDONA, A. & NOSE, A. 2016. A circuit
628 mechanism for the propagation of waves of muscle contraction in Drosophila. *Elife,* 5.
629 GERHARD, S., ANDRADE, I., FETTER, R. D., CARDONA, A. & SCHNEIDER-MIZELL, C. M. 2017.
630 Conserved neural circuit structure across Drosophila larval development revealed by
631 comparative connectomics. *Elife,* 6.
632 GIACHELLO, C., FAN, Y. N., LANDGRAF, M. & BAINES, R. A. 2019. *Activity manipulation of an*
633 *excitatory interneuron, during an embryonic critical period, alters network tuning of the*
634 *Drosophila larval locomotor circuit* [Online]. bioRxiv.org. Available:
635 https://www.biorxiv.org/content/10.1101/780221v1 [Accessed].
636 GIACHELLO, C. N. G., FAN, Y. N., LANDGRAF, M. & BAINES, R. A. 2021. Nitric oxide mediates activity-
637 dependent change to synaptic excitation during a critical period in Drosophila. *Scientific*
638 *Reports,* 11.
639 GROTH, A. C., FISH, M., NUSSE, R. & CALOS, M. P. 2004. Construction of transgenic Drosophila by
640 using the site-specific integrase from phage phi C31. *Genetics,* 166**,** 1775-1782.
641 HASEGAWA, E., TRUMAN, J. W. & NOSE, A. 2016. Identification of excitatory premotor interneurons
642 which regulate local muscle contraction during Drosophila larval locomotion. *Sci Rep,* 6**,**
643 30806.
644 HECKSCHER, E. S., ZARIN, A. A., FAUMONT, S., CLARK, M. Q., MANNING, L., FUSHIKI, A., SCHNEIDER-
645 MIZELL, C. M., FETTER, R. D., TRUMAN, J. W., ZWART, M. F., LANDGRAF, M., CARDONA, A.,
646 LOCKERY, S. R. & DOE, C. Q. 2015. Even-Skipped(+) Interneurons Are Core Components of a
647 Sensorimotor Circuit that Maintains Left-Right Symmetric Muscle Contraction Amplitude.
648 *Neuron,* 88**,** 314-329.
649 HEIMBECK, G., BUGNON, V., GENDRE, N., HABERLIN, C. & STOCKER, R. F. 1999. Smell and taste
650 perception in Drosophila melanogaster larva: Toxin expression studies in chemosensory
651 neurons. *Journal of Neuroscience,* 19**,** 6599-6609.
652 HIRAMOTO, A., JONAITIS, J., NIKI, S., KOHSAKA, H., FETTER, R. D., CARDONA, A., PULVER, S. R. &
653 NOSE, A. 2021. Regulation of coordinated muscular relaxation in Drosophila larvae by a
654 pattern-regulating intersegmental circuit. *Nature Communications,* 12.
655 HOANG, B. & CHIBA, A. 2001. Single-cell analysis of Drosophila larval neuromuscular synapses.
656 *Developmental Biology,* 229**,** 55-70.
657 HUNTER, I., COULSON, B., ZARIN, A. A. & BAINES, R. A. 2021. The Drosophila Larval Locomotor Circuit
658 Provides a Model to Understand Neural Circuit Development and Function. Frontiers in
659 Neural Circuits.
660 ITAKURA, Y., KOHSAKA, H., OHYAMA, T., ZLATIC, M., PULVER, S. R. & NOSE, A. 2015. Identification of
661 Inhibitory Premotor Interneurons Activated at a Late Phase in a Motor Cycle during
662 Drosophila Larval Locomotion. *PLoS One,* 10**,** e0136660.
663 KADAS, D., KLEIN, A., KRICK, N., WORRELL, J. W., RYGLEWSKI, S. & DUCH, C. 2017. Dendritic and
664 Axonal L-Type Calcium Channels Cooperate to Enhance Motoneuron Firing Output during
665 Drosophila Larval Locomotion. *J Neurosci,* 37**,** 10971-10982.
666 KIM, J. H., LEE, S. R., LI, L. H., PARK, H. J., PARK, J. H., LEE, K. Y., KIM, M. K., SHIN, B. A. & CHOI, S. Y.
667 2011. High Cleavage Efficiency of a 2A Peptide Derived from Porcine Teschovirus-1 in Human
668 Cell Lines, Zebrafish and Mice. *Plos One,* 6.

669 KOHSAKA, H., TAKASU, E., MORIMOTO, T. & NOSE, A. 2014. A group of segmental premotor
670 interneurons regulates the speed of axial locomotion in Drosophila larvae. *Curr Biol,* 24**,**
671 2632-42.
672 KOHSAKA, H., ZWART, M. F., FUSHIKI, A., FETTER, R. D., TRUMAN, J. W., CARDONA, A. & NOSE, A.
673 2019. Regulation of forward and backward locomotion through intersegmental feedback
674 circuits in Drosophila larvae. *Nat Commun,* 10**,** 2654.
675 LANDGRAF, M., SANCHEZ-SORIANO, N., TECHNAU, G. M., URBAN, J. & PROKOP, A. 2003. Charting
676 the Drosophila neuropile: a strategy for the standardised characterisation of genetically
677 amenable neurites. *Developmental Biology,* 260**,** 207-225.
678 LARDERET, I., FRITSCH, P. M., GENDRE, N., NEAGU-MAIER, G. L., FETTER, R. D., SCHNEIDER-MIZELL, C.
679 M., TRUMAN, J. W., ZLATIC, M., CARDONA, A. & SPRECHER, S. G. 2017. Organization of the
680 Drosophila larval visual circuit. *Elife,* 6.
681 MARLEY, R. & BAINES, R. A. 2011. Dissection of first- and second-instar Drosophila larvae for
682 electrophysiological recording from neurons: the flat (or fillet) preparation. *Cold Spring Harb*
683 *Protoc,* 2011.
684 OHYAMA, T., SCHNEIDER-MIZELL, C. M., FETTER, R. D., ALEMAN, J. V., FRANCONVILLE, R., RIVERA-
685 ALBA, M., MENSH, B. D., BRANSON, K. M., SIMPSON, J. H., TRUMAN, J. W., CARDONA, A. &
686 ZLATIC, M. 2015. A multilevel multimodal circuit enhances action selection in Drosophila.
687 *Nature,* 520**,** 633-U107.
688 PFEIFFER, B. D., NGO, T. T. B., HIBBARD, K. L., MURPHY, C., JENETT, A., TRUMAN, J. W. & RUBIN, G.
689 M. 2010. Refinement of Tools for Targeted Gene Expression in Drosophila. *Genetics,* 186**,**
690 735-U488.
691 PFEIFFER, B. D., TRUMAN, J. W. & RUBIN, G. M. 2012. Using translational enhancers to increase
692 transgene expression in Drosophila. *Proceedings of the National Academy of Sciences of the*
693 *United States of America,* 109**,** 6626-6631.
694 POTTER, C. J., TASIC, B., RUSSLER, E. V., LIANG, L. & LUO, L. Q. 2010. The Q System: A Repressible
695 Binary System for Transgene Expression, Lineage Tracing, and Mosaic Analysis. *Cell,* 141**,**
696 536-548.
697 REN, D., NAVARRO, B., XU, H., YUE, L., SHI, Q. & CLAPHAM, D. E. 2001. A prokaryotic voltage-gated
698 sodium channel. *Science,* 294**,** 2372-5.
699 ROHRBOUGH, J. & BROADIE, K. 2002. Electrophysiological analysis of synaptic transmission in central
700 neurons of Drosophila larvae. *J Neurophysiol,* 88**,** 847-60.
701 RYGLEWSKI, S., LANCE, K., LEVINE, R. B. & DUCH, C. 2012. Ca(v)2 channels mediate low and high
702 voltage-activated calcium currents in Drosophila motoneurons. *The Journal of physiology,*
703 590**,** 809-25.
704 SAALFELD, S., CARDONA, A., HARTENSTEIN, V. & TOMANCAK, P. 2009. CATMAID: collaborative
705 annotation toolkit for massive amounts of image data. *Bioinformatics,* 25**,** 1984-6.
706 SALES, E. C., HECKMAN, E. L., WARREN, T. L. & DOE, C. Q. 2019. Regulation of subcellular dendritic
707 synapse specificity by axon guidance cues. *Elife,* 8.
708 SAUMWEBER, T., ROHWEDDER, A., SCHLEYER, M., EICHLER, K., CHEN, Y. C., ASO, Y., CARDONA, A.,
709 ESCHBACH, C., KOBLER, O., VOIGT, A., DURAIRAJA, A., MANCINI, N., ZLATIC, M., TRUMAN, J.
710 W., THUM, A. S. & GERBER, B. 2018. Functional architecture of reward learning in mushroom
711 body extrinsic neurons of larval Drosophila. *Nat Commun,* 9**,** 1104.
712 SCHNEIDER-MIZELL, C. M., GERHARD, S., LONGAIR, M., KAZIMIERS, T., LI, F., ZWART, M. F.,
713 CHAMPION, A., MIDGLEY, F. M., FETTER, R. D., SAALFELD, S. & CARDONA, A. 2016.
714 Quantitative neuroanatomy for connectomics in Drosophila. *Elife,* 5.
715 SRINIVASAN, S., LANCE, K. & LEVINE, R. B. 2012a. Contribution of EAG to excitability and potassium
716 currents in Drosophila larval motoneurons. *Journal of neurophysiology,* 107**,** 2660-71.
717 SRINIVASAN, S., LANCE, K. & LEVINE, R. B. 2012b. Segmental differences in firing properties and
718 potassium currents in Drosophila larval motoneurons. *Journal of neurophysiology,* 107**,**
719 1356-65.

SUZUKI, Y., SCHENK, J. E., TAN, H. & GAUDRY, Q. 2020. A Population of Interneurons Signals Changes in the Basal Concentration of Serotonin and Mediates Gain Control in the Drosophila Antennal Lobe. *Current Biology,* 30**,** 1110-+.

WORRELL, J. W. & LEVINE, R. B. 2008. Characterization of voltage-dependent Ca2+ currents in identified Drosophila motoneurons in situ. *J Neurophysiol,* 100**,** 868-78.

YOSHIKAWA, S., LONG, H. & THOMAS, J. B. 2016. A subset of interneurons required for Drosophila larval locomotion. *Molecular and Cellular Neuroscience,* 70**,** 22-29.

ZARIN, A. A., MARK, B., CARDONA, A., LITWIN-KUMAR, A. & DOE, C. Q. 2019. A multilayer circuit architecture for the generation of distinct locomotor behaviors in Drosophila. *Elife,* 8.

ZHANG, X. & GAUDRY, Q. 2018. Examining Monosynaptic Connections in Drosophila Using Tetrodotoxin Resistant Sodium Channels. *J Vis Exp*.

ZHANG, X. N. & GAUDRY, Q. 2016. Functional integration of a serotonergic neuron in the Drosophila antennal lobe. *Elife,* 5.

ZWART, M. F., PULVER, S. R., TRUMAN, J. W., FUSHIKI, A., FETTER, R. D., CARDONA, A. & LANDGRAF, M. 2016. Selective Inhibition Mediates the Sequential Recruitment of Motor Pools. *Neuron,* 91**,** 615-28.

Figure 1. TERPS tool mechanism

(A-B) *UAS-Channelrhodopsin* (ChR) and *UAS-NaChBac* (NaChBac) expression are driven by a Gal4 line, in premotor interneurons (PMIN A and B). (A) Light stimulation of ChR in PMIN A increases its open probability so that an inward, nonspecific cation current depolarises the cell. This depolarisation gates the voltage sensitive NaChBac channel, which carries a strongly depolarising sodium current. This induces synaptic transmission to neighbouring aCC. (B) PMIN B expresses ChR and NaChBac, however, it is not monosynaptically connected to aCC; it is polysynaptically connected to the motoneuron, via PMIN C. TTX blocks the Na_v channels in PMIN C, so that there is no synaptic transmission between it and aCC, following optogenetic stimulation of PMIN B.

Figure 2. Gal4 line expression

(A) *R36G02*-Gal4 ("A27h-Gal4") is expressed in several cell types, including A27h. (B) *15B07*-Gal4 ("CLI2-Gal4"), is specific to A18a (CLI2) interneurons. (C) *R78F07*-AD*; R49C08*-DBD is predominantly expressed in thoracic segments of the VNC and appears to be specific to A23a. (D) *R41G07*-AD*; R78F07*-DBD, a.k.a. *SS04495*-Gal4, is expressed in abdominal segments of the VNC and also appears to be specific to A23a. Note that in contrast to these images, our electrophysiology and pharmacology suggested neither *R78F07*-AD*; R49C08*-DBD, nor *SS04495*-Gal4, was specific to A23a. (E) *R20A03*-AD*; R93B07*-DBD, a.k.a. *SS04399*-Gal4, is strongly expressed in only the most

posterior abdominal segments of the VNC, and is specific to A31k interneurons. All expression patterns were imaged 48h AEL. Left-hand panels show merged images, while right-hand panels show an enlarged, GFP channel only section of left panel (indicated by dotted square bracket) that highlights individual neurons.

Figure 3. *ChR; NaChBac* is a powerful tool to verify monosynaptic connectivity

(A) A representative current-clamp recording from the A27h IN overexpressing both ChR and NaChBac. Optogenetic stimulation (λ470 nm, 1 s) induced activation of NaChBac which persists in the presence of 2μM TTX (arrowheads). Conversely, APs produced by activation of endogenous voltage-gated sodium channels were blocked after TTX application (arrows). (B) Voltage dependence of NaChBac activation recorded from A27h in current-clamp. A27h depolarisation was elicited by injecting constant current steps (1pA steps/0.5s, V_m = -90mV) in the presence of TTX. (C-D) Voltage-dependent inactivation of NaChBac. Peak amplitude was recorded and measured from A27h held at different prepulse voltages (from -90 to -20mV) during optogenetic stimulation (470nm, 1s). NaChBac activation is reduced at V_m more positive than -40mV. Note: there is a second activation (peak) of NaChBaC at -90mV. (D) Averaged data ± SEM (n = 3) for traces shown in C. (E) Sample recording of synaptic drive to aCC, recorded in voltage-clamp, following optogenetic activation of A27h (470nm, 1 s). In presence of TTX, co-expression and activation of both ChR and NaChBac in A27h produced a clear synaptic input in aCC (inward current, black trace), thus confirming the existence of a monosynaptic connection between these two neurons. As a control, TTX successfully blocked aCC inputs when only ChR, but not NaChBac, was expressed in A27h (red trace). These results validate that A27h is monosynaptically connected to aCC and validate the use of ChR; NaChBac to identify other monosynaptically-connected neuron pairs.

Figure 4. A18a, but not A18b3, is monosynaptically connected to the aCC motoneuron

(A-B) Excitatory synaptic inputs to aCC recorded in absence (A) and presence of TTX (B and inset). Four different Gal4 lines were used to target ChR and NaChBac expression to the CLI interneurons,

780 A18a and A18b3. (C) Quantification of aCC synaptic drive revealed that A18a, but not A18b3, is
781 monosynaptically connected to aCC. The TTX-induced reduction, but not elimination, of synaptic
782 current amplitudes in some Gal4 expression lines (e.g. *R47E12*-Gal4 ("CLIs-Gal4")) suggests the
783 presence of additional Gal4-expressing interneurons not directly connected the aCC motoneuron, but
784 indirectly contributing to its overall excitation following optogenetic stimulation in absence of TTX.

785 **Figure 5. aCC motoneurons receive inputs from GABAergic interneurons**

786 (A) Sample trace and quantification of APs evoked by injecting a supra-threshold depolarising current
787 into aCC. Optogenetic activation of all GABAergic interneurons (*GAD1-T2A*-Gal4>*UAS- T159C-*
788 *ChR*, 470nm, 1s) almost completely inhibited AP firing in aCC (*n* = 7, black lines), clearly showing
789 that aCC receives inhibitory inputs. Average values are shown in red. (B-C) Sample trace and
790 quantification of the inhibitory drive to aCC recorded in voltage-clamp mode. The same cells were
791 recorded at V_m of -40 and -60mV. As expected, we observed a large outward current (at -40mV)
792 which attenuated at more negative potentials (-60mV) close to the chloride reversal potential (approx.
793 -70mV). (D-E) Sample trace and quantification of the inhibitory drive to aCC recorded in current-
794 clamp mode showing a clear hyperpolarisation of aCC and similar attenuation at -60mV compared to
795 -40mV.

796 **Figure 6. A23a and aCC are monosynaptically connected**

797 (A) Optogenetic activation of *R78F07*-Gal4 driving ChR; NaChBac reduces AP firing in aCC
798 (elicited by injection of constant current). On average, we observed an inhibitory effect (*n* = 6, black
799 lines). Average values are shown in red. (B) Quantification of the synaptic inputs recorded from aCC
800 (V_m -40mV) following optogenetic activation of *R78F07*-Gal4 driving ChR; NaChBac, before and
801 after 2µM TTX application. In the presence of TTX, we observed a heterogeneous range of inputs
802 with excitation prevailing over inhibition. Some recordings (2 out of 8 cells) showed a biphasic
803 connection where both the excitatory and inhibitory components were observed in the same cell
804 (values highlighted with a different colour, +TTX group). (C) Raw electrophysiological sweeps from
805 an example of a biphasic connection obtained with optogenetic activation of *R78F07*-Gal4. The same

806 cell was recorded 5 times during optogenetic stimulation before (black traces) and after (red traces)
807 TTX exposure. Whilst the inhibitory component seems to prevail before applying TTX, isolation of
808 NaChBac -overexpressing neurons (+TTX) resulted in a reliable excitatory component (arrowhead)
809 followed by a delayed erratic inhibitory component (arrow). (D) Optogenetic activation of *R78F07-*
810 AD*; R49C08*-DBD split Gal4 did not affect aCC firing (*n* = 8, black lines). Average values are shown
811 in red. (E) Optogenetic activation of *R41G07*-AD*; R78F07*-DBD split Gal4 significantly reduced aCC
812 firing (*n* = 8, black lines). Average values are shown in red. (F) Quantification of the synaptic drive to
813 aCC (V_m -40mV) following optogenetic activation of *R41G07*-AD*; R78F07*-DBD split Gal4 in the
814 absence, or presence, of 2µM TTX. The prevalence of inhibitory inputs suggests a better specificity
815 for this line in targeting A23a compared to previous tested lines. (G) Sample traces showing the
816 optogenetic activation of *R41G07*-AD*; R78F07*-DBD split Gal4, driving ChR; NaChBac. aCC were
817 recorded both in voltage- (both at -60 and -40mV) and in current clamp (at -40mV) in presence of
818 TTX. (H-I) Sample traces confirming that the A23a→ aCC synapse is GABAergic. Cells were
819 recorded, as previously described, before (black trace) and after (grey trace) bath application of 10µM
820 picrotoxin (H) or 1mM gabazine (I), two blockers of the *Drosophila* $GABA_A$ receptor. In both cases,
821 aCC inputs were abolished.

822 **Figure 7. A31k and aCC are monosynaptically connected**

823 (A-B) Optogenetic activation of *R20A03*-AD*; R87H09*-DBD split Gal4, did not produce detectable
824 changes in aCC firing (evoked by current injection) recorded at both (A) L3 (*n* = 3, black lines), and
825 (B) L1 (*n* = 5, black lines). Average values are shown in red. (C) Optogenetic activation of *R20A03-*
826 AD*; R93B07*-DBD split Gal4 significantly reduced aCC firing (*n* = 5, black lines). Average values are
827 shown in red. (D) Quantification of the synaptic drive to aCC (V_m -40mV) following optogenetic
828 activation of *R20A03*-AD*; R93B07*-DBD split Gal4, in absence or presence of 2µM TTX. (E) Sample
829 traces showing the optogenetic activation of *R20A03*-AD*; R93B07*-DBD split Gal4. aCC neurons
830 were recorded both in voltage (V_m -60 and -40mV) and in current-clamp (-40mV) configurations, in
831 the presence of TTX. (F-G) Sample traces confirming the GABAergic connection between A31k and

aCC. Cells were recorded, as previously described, before (black trace) and after (grey trace) the bath application of 10µM picrotoxin (F), or 1mM gabazine (G). In both cases, aCC inputs were abolished.

Figure 8: GFP Reconstitution across Synaptic Partners (GRASP) is not specific to direct synaptic partners

(A-F) Three-color fluorescence imaging of nerve cords 72 hours after larval hatching, to examine cerulean-GRASP signal between aCC and RP2 motoneurons with two different premotor interneurons: A18a (a.k.a. CLI2) and A18b3 (a.k.a. CLI1). A and D show overlays of fluorescence with brightfield illumination taken with a 10X objective, providing an overview of the whole nerve cord, with the dashed white line indicating the region imaged with 60X objective, shown to the right (B and E). The dashed white boxes in B and E (aCC dendritic regions) outline regions magnified in panels C and F. (A-C) *15B07*-Gal4 drives expression of *UAS-CD4::tdTomato* in A18a interneurons (red). (D-F) *tsh*-Gal80*; R47E12*-Gal4*, Cha3.3*-Gal80 targets expression of *UAS-CD4::tdTomato* to A18b3 interneurons (red). (A-F) Subsets of aCC were stochastically labelled with *LexAop2-myr::YPet* (yellow) via Flippase (Dhawan et al., 2021) expressed in those neurons. Cell-cell contacts are visualized using a cyan version of GRASP, *UAS-CD4::spCerulean1-10*, expressed by the respective interneurons, while the complementary *LexAop-CD4::spGFP11* is expressed in subsets of aCC. At points of sufficient proximity between cell pairs, cerulean fluorescent protein is reconstituted (cyan). Robust cerulean fluorescence is detected using both A18a and A18b3 Gal4 drivers, at contact sites with aCC.

Figure 9. A TERPS and RCaMP imaging tool can identify excitatory monosynaptic connections between cells

(A) representative trace showing optogenetic activation of A27h expressing NaChBac, in the presence of 2µM TTX, induces a clear change in calcium levels (indicated by a change in RCaMP fluorescence) in aCC (~200AU above base line, $n = 5$). Addition of the cholinergic blocker, mecamylamine (200µM), to the same preparation abolishes this response (right-hand panel). All that remains is a smaller light-induced artifact due to the activation of the blue LED. (B) Representative

858 trace for optogenetic activation of A31k expressing NaChBac, in the presence of 2μM TTX, shows
859 that activation of this premotor interneuron does alter calcium levels in aCC (no change in AU above
860 base line, besides the peak explained in C, *n* = 5). (C) Representative trace for flashing Canton-S
861 wild-type larvae, showing that it is light from the blue LED that produces the recording artifact
862 (arrowhead, *n* = 1).

863 **Figure 10. aCC-associated circuit connectivity**

864 Schematic showing relationship between the cholinergic (A27h, A18b3 and A18a) and GABAergic
865 (A23a and A31k) premotor interneurons we tested for monosynaptic connectivity to the motoneuron,
866 aCC. Arrows depict synapses with connectivity verified by electrophysiology. Traces to the right of
867 the schematic are representative examples of the effect of cholinergic and GABAergic monosynaptic
868 inputs on evoked action potentials aCC, taken from recordings from A27h and A31k stimulation,
869 respectively.

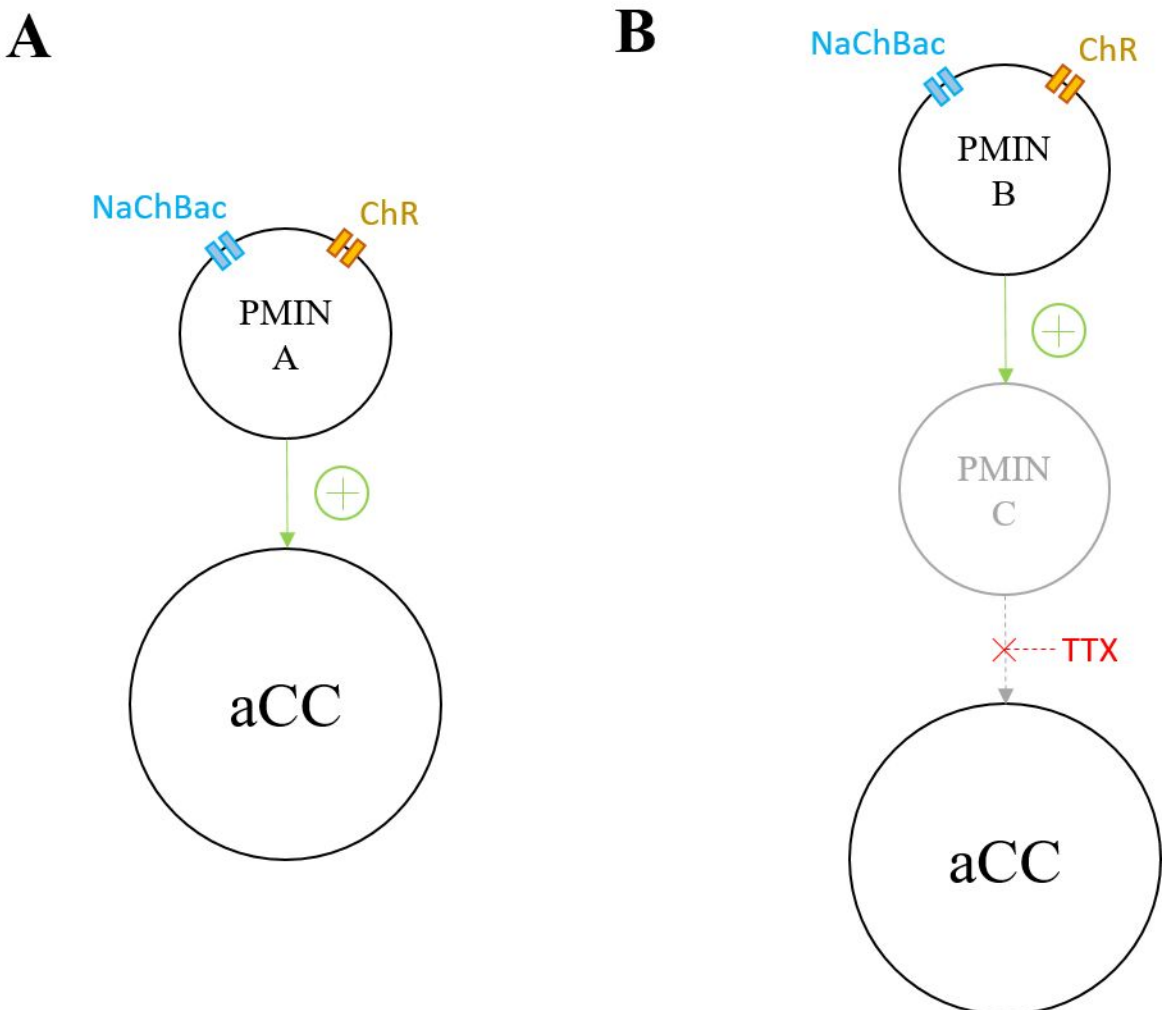
A
NaChBac
ChR
PMIN
A
aCC
B
NaChBac
ChR
PMIN
B
PMIN
C
TTX
aCC

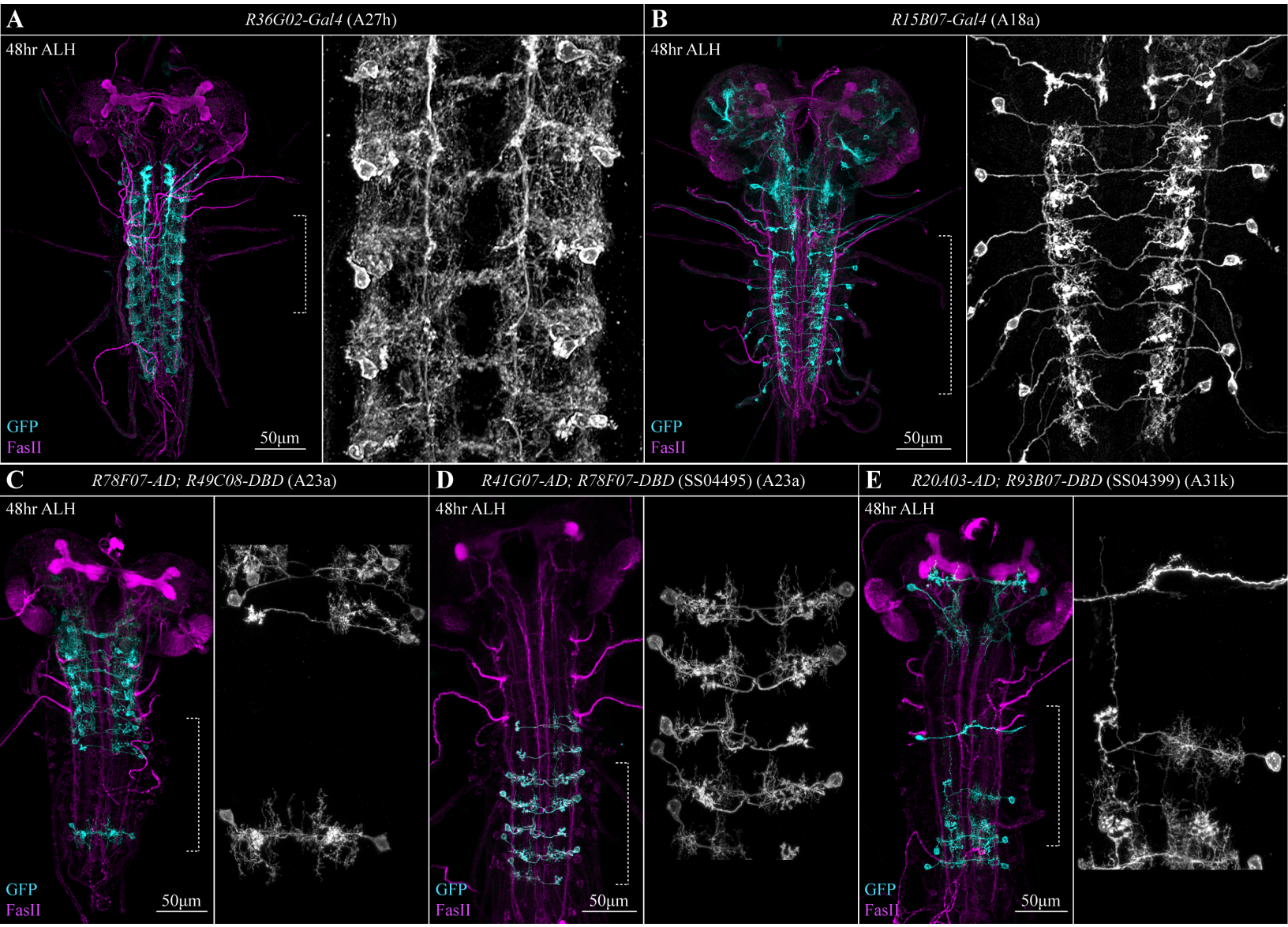
A
R36G02-Gal4 (A27h)
48hr ALH
GFP
FasII
50µm
B
R15B07-Gal4 (A18a)
48hr ALH
GFP
FasII
50µm
C
R78F07-AD; R49C08-DBD (A23a)
48hr ALH
GFP
FasII
50µm
D
R41G07-AD; R78F07-DBD (SS04495) (A23a)
48hr ALH
GFP
FasII
50µm
E
R20A03-AD; R93B07-DBD (SS04399) (A31k)
48hr ALH
GFP
FasII
50µm

Figure 1

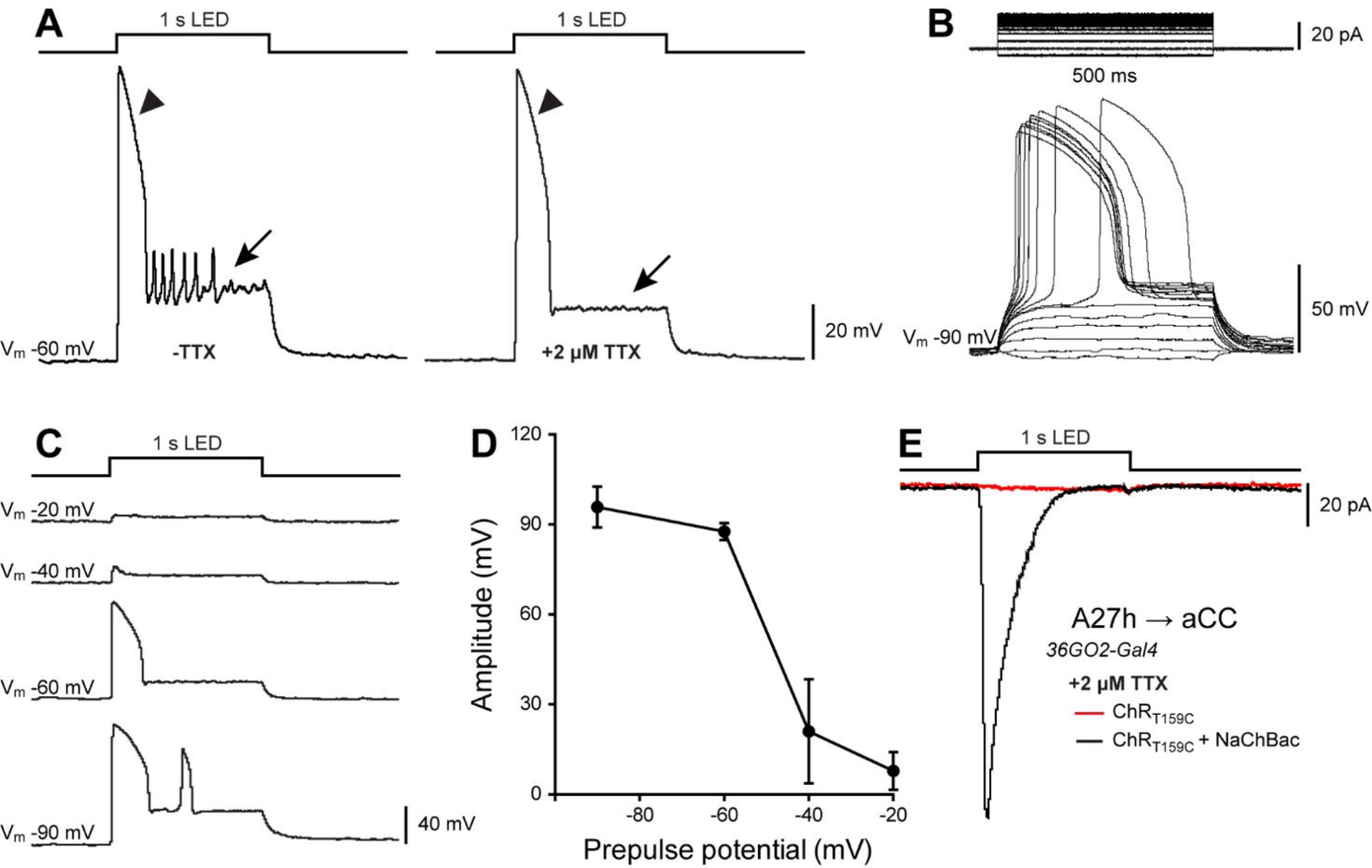
A
1 s LED
1 s LED
Vm -60 mV
-TTX
+2 μM TTX
20 mV
B
20 pA
500 ms
50 mV
Vm -90 mV
C
1 s LED
Vm -20 mV
Vm -40 mV
Vm -60 mV
Vm -90 mV
40 mV
D
Amplitude (mV)
120
90
60
30
0
-80
-60
-40
-20
Prepulse potential (mV)
E
1 s LED
20 pA
A27h → aCC
36GO2-Gal4
+2 μM TTX
ChRT159C
ChRT159C + NaChBac

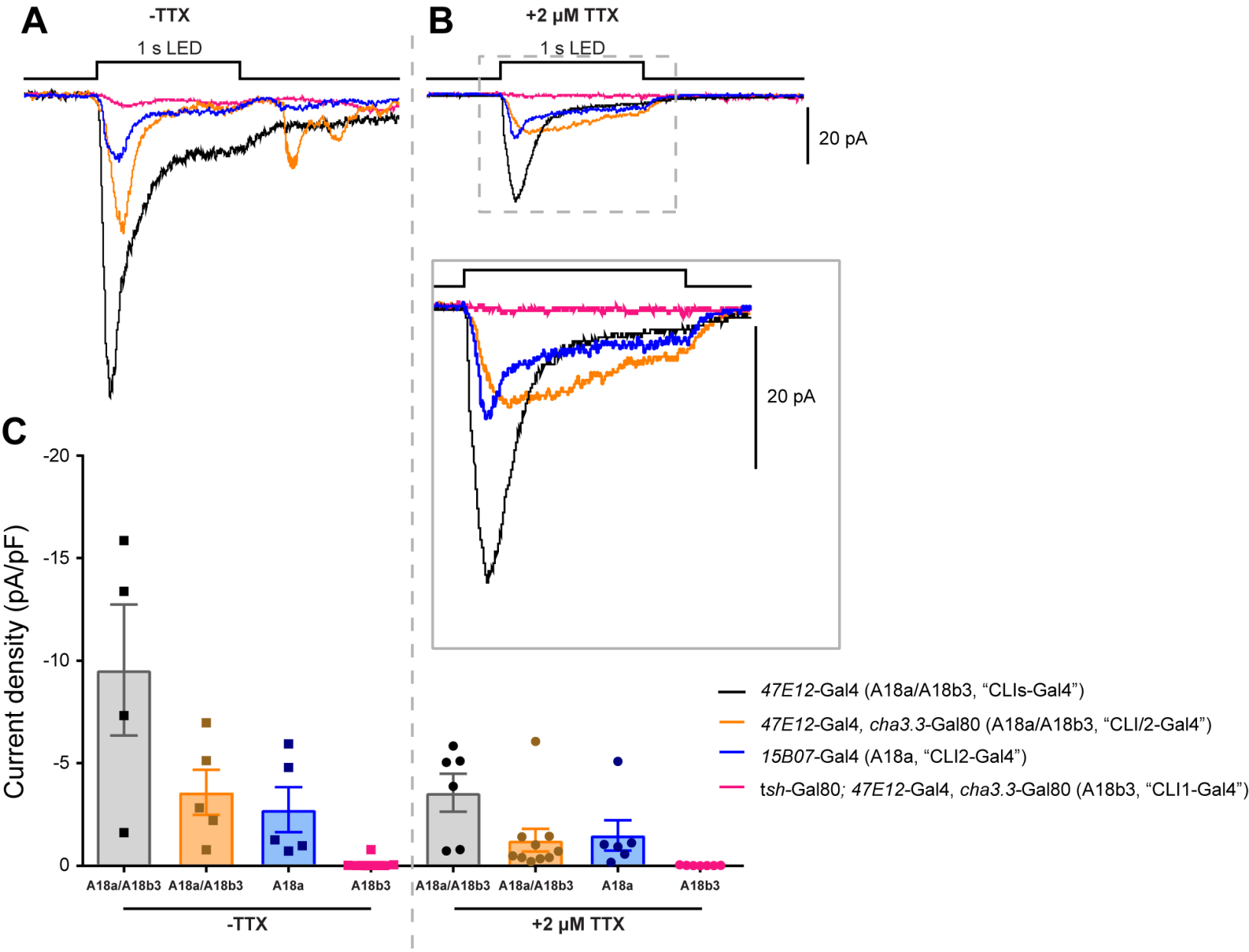
A
-TTX
1 s LED
B
+2 µM TTX
1 s LED
20 pA
20 pA
C
Current density (pA/pF)
-20
-15
-10
-5
0
A18a/A18b3
A18a/A18b3
A18a
A18b3
A18a/A18b3
A18a/A18b3
A18a
A18b3
-TTX
+2 µM TTX
47E12-Gal4 (A18a/A18b3, "CLIs-Gal4")
47E12-Gal4, cha3.3-Gal80 (A18a/A18b3, "CLI/2-Gal4")
15B07-Gal4 (A18a, "CLI2-Gal4")
tsh-Gal80; 47E12-Gal4, cha3.3-Gal80 (A18b3, "CLI1-Gal4")

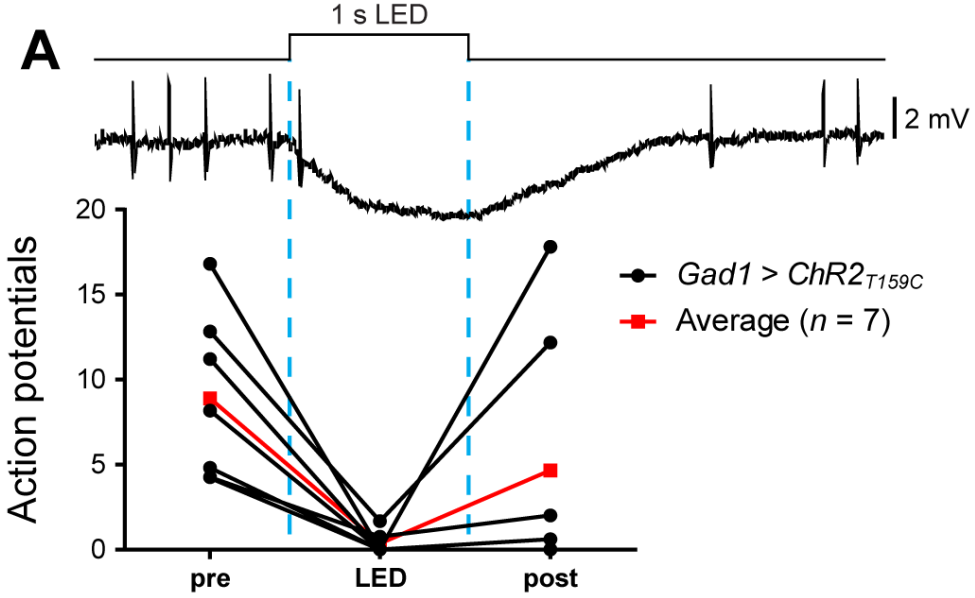
A
1 s LED
2 mV
Action potentials
20
15
10
5
0
pre
LED
post
Gad1 > ChR2T159C
Average (n = 7)

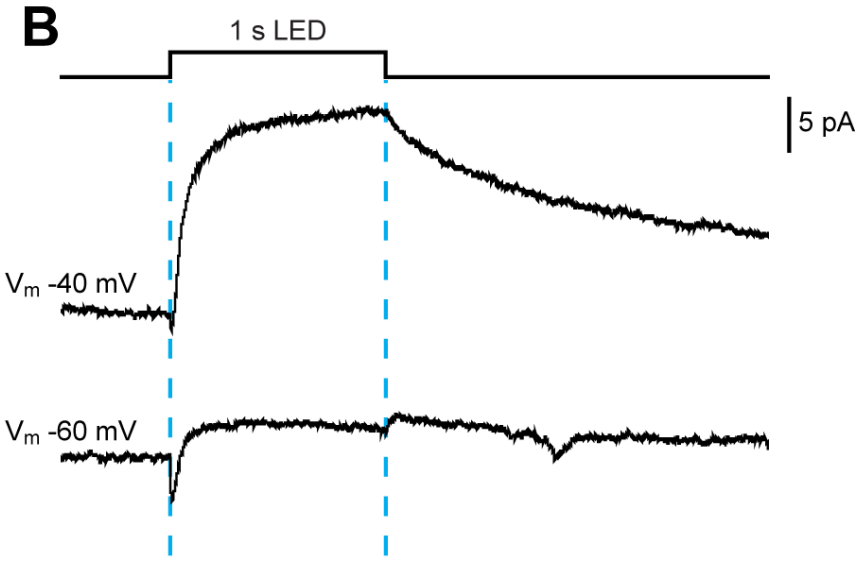
B
1 s LED
5 pA
Vm -40 mV
Vm -60 mV

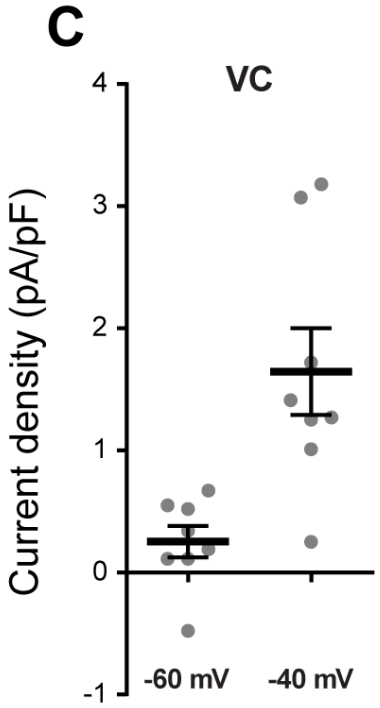
C
VC
Current density (pA/pF)
4
3
2
1
0
-1
-60 mV
-40 mV

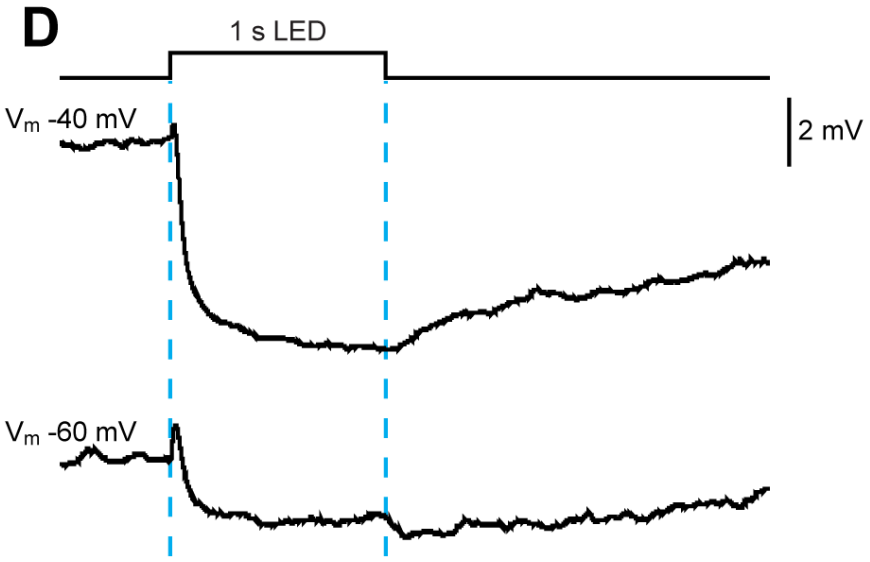
D
1 s LED
Vm -40 mV
2 mV
Vm -60 mV

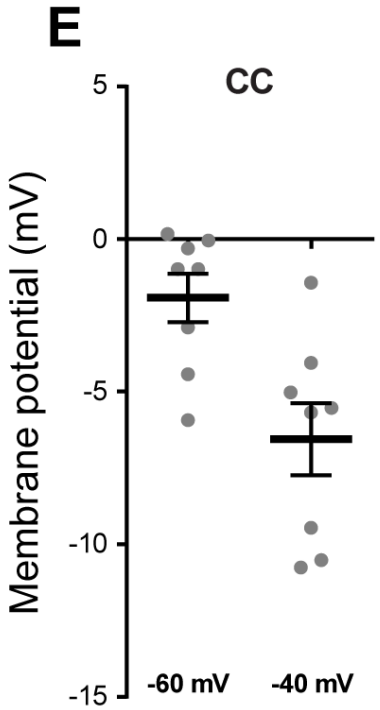
E
CC
Membrane potential (mV)
5
0
-5
-10
-15
-60 mV
-40 mV

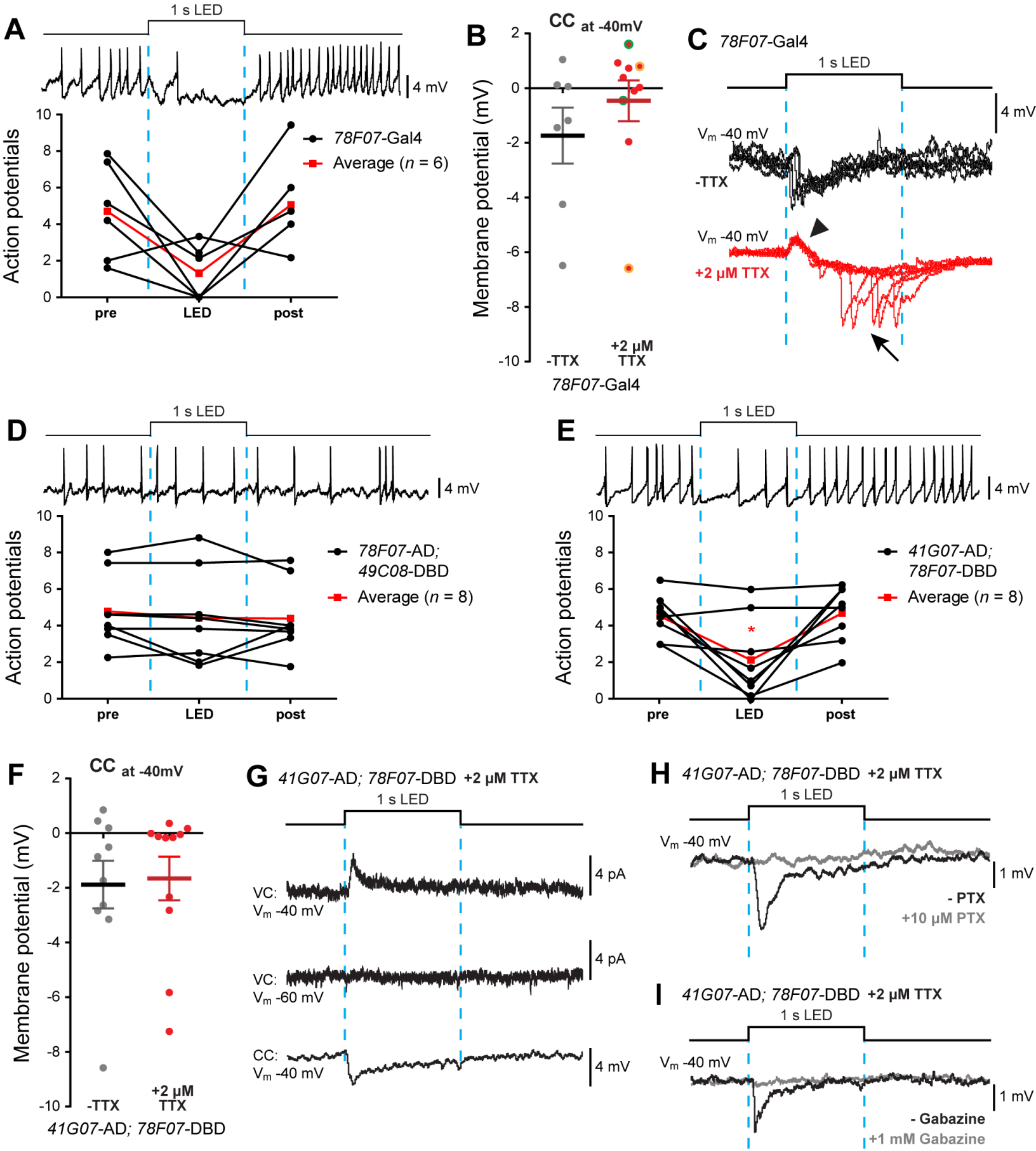
A
1 s LED
4 mV
Action potentials
78F07-Gal4
Average (n = 6)
pre
LED
post
B
CC at -40mV
Membrane potential (mV)
-TTX
+2 μM TTX
78F07-Gal4
C
78F07-Gal4
1 s LED
4 mV
Vm -40 mV
-TTX
Vm -40 mV
+2 μM TTX
D
1 s LED
4 mV
Action potentials
78F07-AD; 49C08-DBD
Average (n = 8)
pre
LED
post
E
1 s LED
4 mV
Action potentials
41G07-AD; 78F07-DBD
Average (n = 8)
pre
LED
post
F
CC at -40mV
Membrane potential (mV)
-TTX
+2 μM TTX
41G07-AD; 78F07-DBD
G
41G07-AD; 78F07-DBD +2 μM TTX
1 s LED
VC: Vm -40 mV
4 pA
VC: Vm -60 mV
4 pA
CC: Vm -40 mV
4 mV
H
41G07-AD; 78F07-DBD +2 μM TTX
1 s LED
Vm -40 mV
1 mV
- PTX
+10 μM PTX
I
41G07-AD; 78F07-DBD +2 μM TTX
1 s LED
Vm -40 mV
1 mV
- Gabazine
+1 mM Gabazine

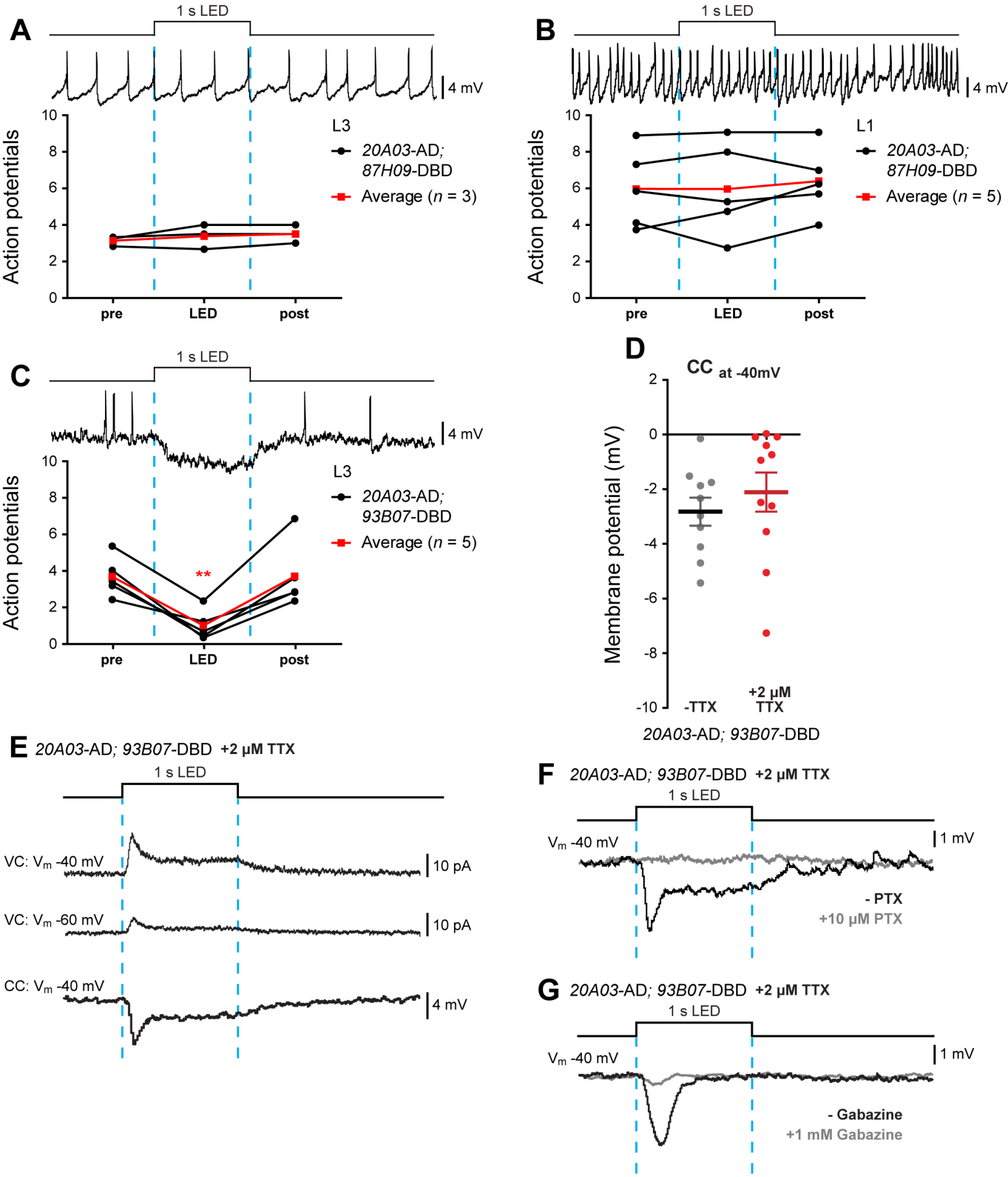
A
1 s LED
4 mV
Action potentials
L3
20A03-AD; 87H09-DBD
Average (n = 3)
pre
LED
post
B
1 s LED
4 mV
Action potentials
L1
20A03-AD; 87H09-DBD
Average (n = 5)
pre
LED
post
C
1 s LED
4 mV
Action potentials
L3
20A03-AD; 93B07-DBD
Average (n = 5)
**
pre
LED
post
D
CC at -40mV
Membrane potential (mV)
-TTX
+2 µM TTX
20A03-AD; 93B07-DBD
E 20A03-AD; 93B07-DBD +2 µM TTX
1 s LED
VC: Vm -40 mV
10 pA
VC: Vm -60 mV
10 pA
CC: Vm -40 mV
4 mV
F 20A03-AD; 93B07-DBD +2 µM TTX
1 s LED
Vm -40 mV
1 mV
- PTX
+10 µM PTX
G 20A03-AD; 93B07-DBD +2 µM TTX
1 s LED
Vm -40 mV
1 mV
- Gabazine
+1 mM Gabazine

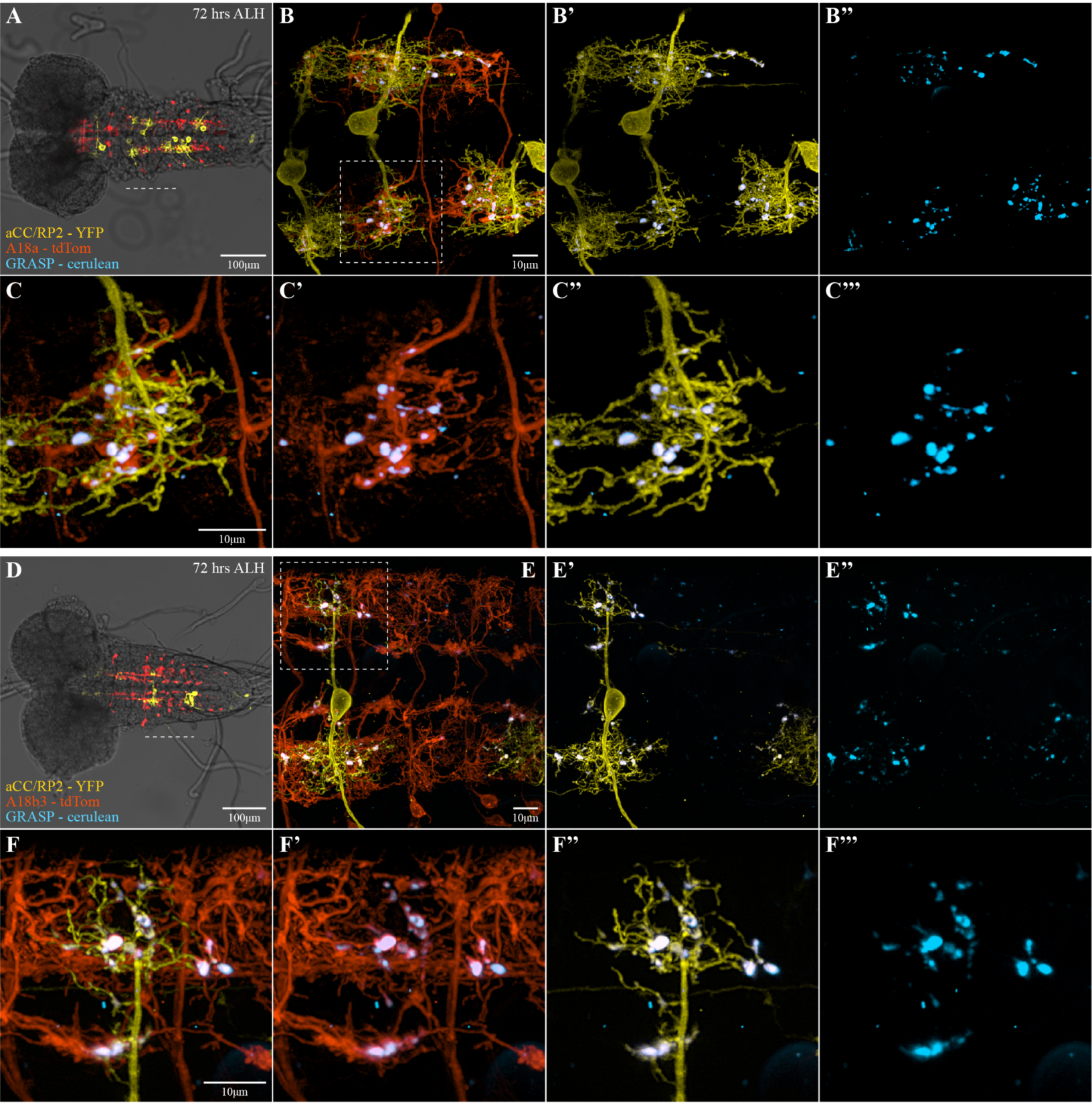
A
72 hrs ALH
aCC/RP2 - YFP
A18a - tdTom
GRASP - cerulean
100µm
B
10µm
B'
B''
C
10µm
C'
C''
C'''
D
72 hrs ALH
aCC/RP2 - YFP
A18b3 - tdTom
GRASP - cerulean
100µm
E
10µm
E'
E''
F
10µm
F'
F''
F'''

A A27h-Gal4 x DvGlut, RCaMP1b, UAS-ChRh; UAS-NaChBac

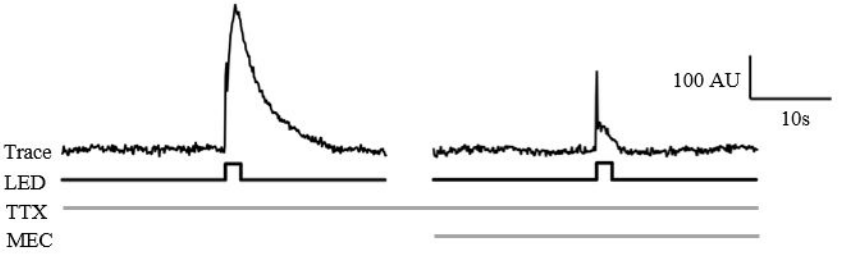

B A31k-Gal4 x DvGlut, RCaMP1b, UAS-ChRh; UAS-NaChBac

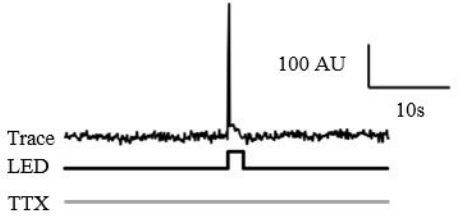

C Canton-S

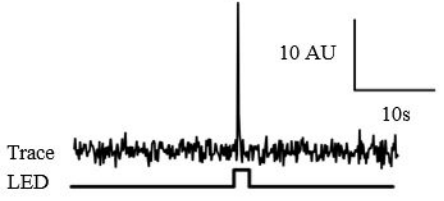

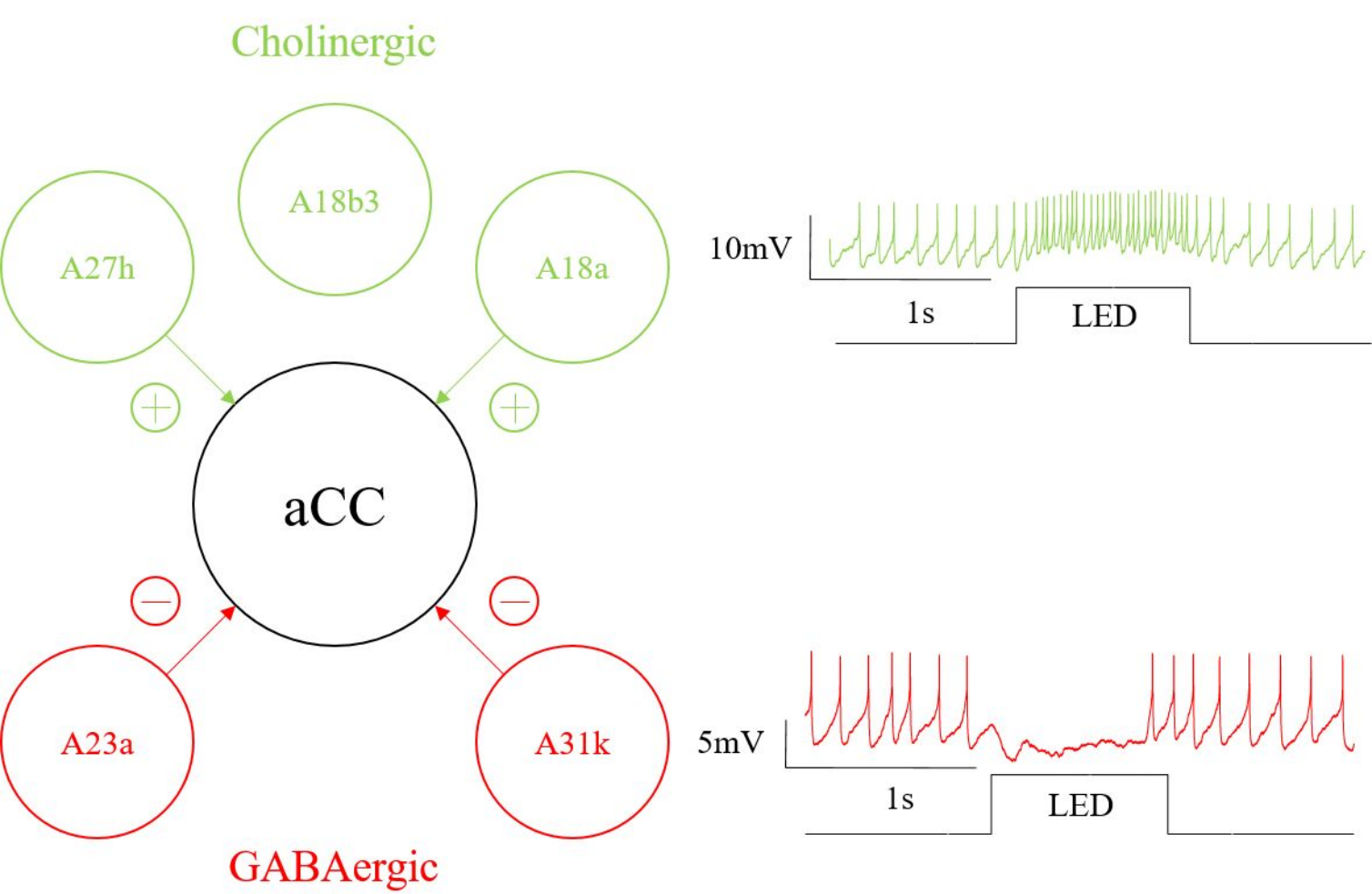
Cholinergic
A18b3
A27h
A18a
aCC
A23a
A31k
GABAergic
10mV
1s
LED
5mV
1s
LED